Received: 12 June 2017 | Revised and accepted: 18 July 2017 | Uncorrected manuscript published: 21 July 2017

DOI: 10.1111/tra.12504

WILEY Traffic

ORIGINAL ARTICLE

Heterogeneity in kinesin function

Babu J.N. Reddy[1] | Suvranta Tripathy[1,2] | Michael Vershinin[3] | Marvin E. Tanenbaum[4] | Jing Xu[5] | Michelle Mattson-Hoss[1] | Karim Arabi[1] | Dail Chapman[1] | Tory Doolin[1] | Changbong Hyeon[6] | Steven P. Gross[1]

[1]Department of Developmental and Cell Biology, University of California, Irvine, CA

[2]Perelman School of Medicine, University of Pennsylvania, Philadelphia, Pennsylvania

[3]Department of Physics and Astronomy, University of Utah, Salt Lake City, Utah

[4]Hubrecht Institute, The Royal Netherlands Academy of Arts and Sciences (KNAW) and University Medical Center, Utrecht, The Netherlands

[5]School of Natural Sciences, University of California, Merced, California

[6]Korea Institute for Advanced Study, Seoul, Korea

Correspondence
Changbong Hyeon, Korea Institute for Advanced Study, Seoul, Korea.
Email: hyeoncb@kias.re.kr
Steven P. Gross, Department of Developmental and Cell Biology, University of California, Irvine, CA.
Email: sgross@uci.edu

The kinesin family proteins are often studied as prototypical molecular motors; a deeper understanding of them can illuminate regulation of intracellular transport. It is typically assumed that they function identically. Here we find that this assumption of homogeneous function appears incorrect: variation among motors' velocities in vivo and in vitro is larger than the stochastic variation expected for an ensemble of "identical" motors. When moving on microtubules, slow and fast motors are persistently slow, and fast, respectively. We develop theory that provides quantitative criteria to determine whether the observed single-molecule variation is too large to be generated from an ensemble of identical molecules. To analyze such heterogeneity, we group traces into homogeneous sub-ensembles. Motility studies varying the temperature, pH and glycerol concentration suggest at least 2 distinct functional states that are independently affected by external conditions. We end by investigating the functional ramifications of such heterogeneity through Monte-Carlo multi-motor simulations.

KEYWORDS

kinesin, kinesin velocity heterogeneity, molecular motors, proteins in glycerol and altered pH, temperature dependence of kinesin motility

1 | INTRODUCTION

Kinesin-family motors play many subcellular roles,[1] and appear adapted to specialized functions with quite different mean velocities and stalling forces, as well as different behavior under load.[2–5] They serve a wide range of cellular roles, and have a central role in creating and maintaining cellular organization—indeed, impaired function is linked to diseases such as neurodegeneration.[6,7] Thus, there is significant interest in achieving a mechanistic understanding of their single-molecule function, and in relating this to ensemble function involving multiple motors.[8–13] In our single-molecule studies of kinesin-1, we observed surprising heterogeneity of function: many motors moved relatively rapidly (~800 nm/s), but some moved significantly slower (eg, ~200 nm/s). We initially ignored this slower population as "unhealthy," and focused on the faster population. However, lacking justification, we later developed assays to allow us to study many more individual motors, and evaluated all active motors. We complemented the increased experimental data with theory, to evaluate how much heterogeneity should be expected from random variation. Once we concluded that the observed variation was in excess to that expected from simple random variation, fitting to theoretical distributions was used to group motors into homogeneous sub-groups. We then explored how different experimental conditions known to affect protein folding might affect partitioning into these subgroups.

As kinesins function in groups, we next wondered about the ramifications of heterogeneity for ensemble function. Previously, several groups had studied the effect of heterogeneous velocities on the group behavior of kinesins, but in those studies, the velocity heterogeneity resulted from having different kinesin family members on the same cargo,[9,11,12] or from induced mutations.[14] Importantly, in our modeling we not only included the amount of heterogeneity observed experimentally but also evaluate how different single-motor detachment assumptions (including one with strong experimental support[5]) affected such ensemble function. In conclusion, here we

describe these combined studies, which lead us to propose that there are at least two distinct functional states of the motors, likely reflecting different folded states. Based on our modeling, we speculate that motors have evolved in order to minimize the functional effects of such heterogeneity, but that the heterogeneity provides a surprising advantage in increasing the probability of the ensemble reaching the steady state.

2 | RESULTS

2.1 | Single kinesin motors exhibit heterogeneity in vitro, attached to beads

When we first examined the motility of full length kinesin-1[15] purified from *Drosophila* embryos, attached non-specifically to carboxylated beads, we observed a variety of velocities of single-motor beads (Figure 1A): some motors appeared to move persistently fast and others persistently slow. Similar variation in velocity was observed in a bead motility assay with bacterially expressed human K-560[16] (Figure 1B). In each case, the heterogeneity was observed in multiple experiments carried out on different days, with K560-gfps purified in different batches (wild-type K560 without a gfp label also showed similar behavior in at least 3 different trials). This truncated kinesin-1, lacks its tail, as well as light chains and post-translational modifications potentially found in full length fly kinesins.

2.2 | Theoretical determination of expected velocity distribution for homogeneous motors

Molecular movement visualized in real-time by single molecule experiments[17–19] allows us to conduct time series analysis on individual molecules, as well as to calculate the distribution of dynamic variables, which are difficult to determine from ensemble averaged measurements. There have been a number of studies reporting heterogeneities (or dynamic/static disorder) over the molecular population.[18,20–25] In such a system with molecular heterogeneity, a dynamic pattern observed in one molecule often differs from that in another, even when molecules of a chemically identical composition are under the same experimental conditions. Formally, enzymes are expected to have (multiple) rate-limiting steps and each kinetic step is stochastic, so it is a priori not obvious whether observed experimental variation simply reflects the stochasticity in rate processes. To address this, we developed a quantitative criteria to determine whether the observed single-molecule variation is greater than the stochastic variation expected for the population of homogeneous motors: the mean velocity $\frac{x(t)}{t} = V(t)$ up to time t should obey the Gaussian-like velocity distribution

$$P_G[V(t)] = \left(\frac{t}{4\pi \overline{D}}\right)^{1/2} \exp\left[-\frac{(V(t)-\overline{V})^2}{4\overline{D}/t}\right] \quad (1)$$

where $\overline{V}$ and $\overline{D}$, in fact, can be expressed in terms of a single parameter τ as $\overline{V}\left(=\frac{d}{\tau}=0.8\,\mu m/s\right)$ and $\overline{D}=d^2/2\tau\left(=0.0032\,\mu m^2/s\right)$; see

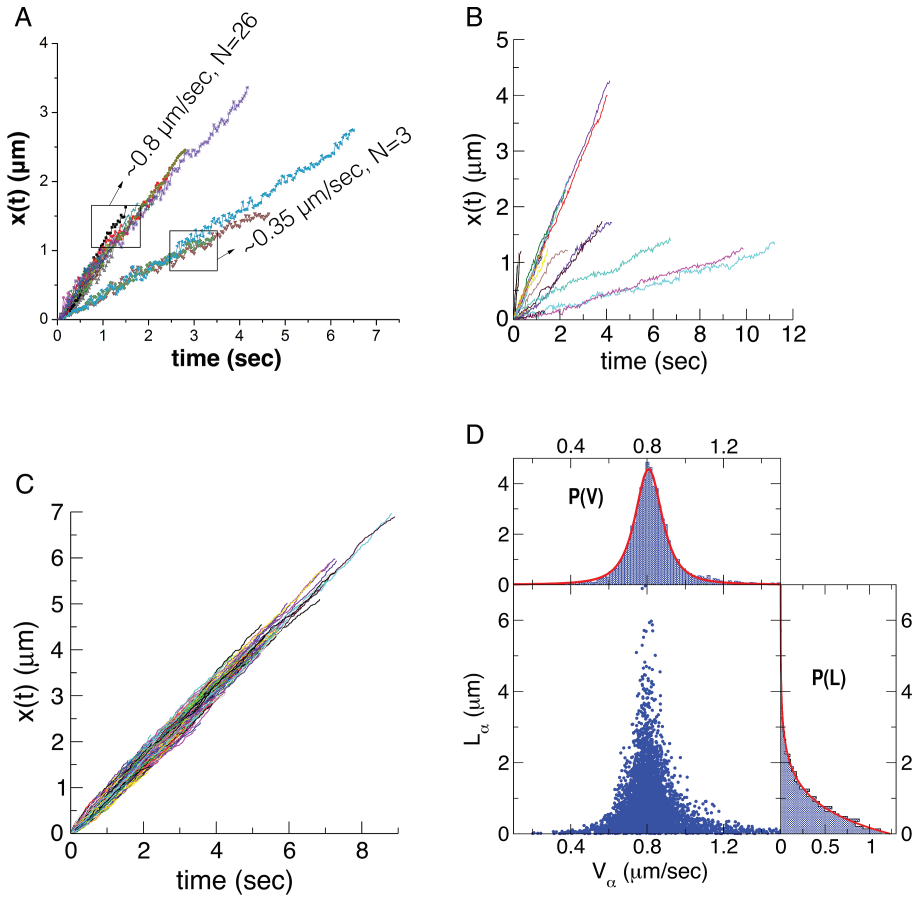

FIGURE 1 Time traces of single kinesin motors in vitro. A, Displacements of beads moved by single kinesin motors purified from Drosophila embryos, where 2 subpopulations of mean velocities (0.8 microns/sec [N = 26] and 0.35 microns/sec [N = 3] are observed. B, K560 expressed in *Escherichia coli*, from bead assays (N = 32). The motors' tail is specifically attached to the bead through streptavidin-biotin with 30% of kinesin/bead binding fraction. C, Computer generated time traces (N = 5000) with $\Psi(t) = \tau^{-1}e^{-t/\tau}$ (τ = 10 ms) and detachment probability of P = .01 at each step. D, The histogram of travel distance (right panel) is fitted to $P(L) = \overline{L}^{-1}e^{-L/\overline{L}}$ with $\overline{L} = 0.8\,\mu m$ (red line); and the velocity distribution (top panel) to Equation 3 with $\overline{D} = 0.0033\,\mu m^2/s$ $\overline{V} = 0.8\,\mu m/sec$ and $\overline{L} = 0.8\,\mu m$ (red line)

supplement for derivation, and full discussion. Importantly, for Poisson walkers such as kinesin, the relative error in the mean velocity is expected to scale with the number of steps (n) as

$$\frac{\alpha_v}{\overline{V}} \sim \frac{1}{\sqrt{n}} \tag{2}$$

which is because $\sqrt{\alpha_V^2}/\overline{V} = (2\overline{D}/t)^{1/2}/\overline{V} = \sqrt{\tau/t} = \sqrt{1/n}$. Thus, when n = 100 (ie, for runs ~800-nm long), the relative error in velocity is expected to be 10%, that is, the mean velocity calculated for the ensemble of walkers that have taken n = 100 steps should tightly fit in the range of $V_{n\,=\,100}$ = 0.8 ± 0.08 μm/s. This is indeed what the simulated stochastic walkers show (Figure 1C,D), but it is obviously far less disperse than what we are observing for the experiments (Figure 1A,B).

2.3 | Velocity distribution for motors with a finite processivity

In practice, kinesin motors have a finite processivity with an exponential travel time distribution, $p_{\overline{L}}(t) = (\overline{V}/\overline{L})e^{-\overline{V}t/\overline{L}}$, as is the case in our simulation data, where a finite detachment probability (p = .01, which amounts to the dissociation rate of $k_{\text{diss}} = p/\tau = \overline{V}/\overline{L} = 1\,s^{-1}$ is imposed on each step of Poisson walkers (see Figure 1C).

Then, for an ensemble of homogeneous motors with exponential travel distance, the distribution of mean velocities ought to be described by incorporating the travel time distribution as a weighting factor, which leads to

$$P_{\text{homo}}(V;\overline{V},\overline{D},\overline{L}) = \int_0^\infty dt P_G[V(t)]P_{\overline{L}}(t) = \frac{\overline{V}/\overline{L}}{4\sqrt{\overline{D}}}\left[\frac{(V-\overline{V})^2}{4\overline{D}} + \frac{\overline{V}}{\overline{L}}\right]^{-3/2} \tag{3}$$

Note that Equation 3 is symmetric with respect to $\overline{V}$ and has a single peak and power-law tails at both ends. It is of particular note that from the scatter plot of (V_α, L_α), which depicts the mean velocity and run-length from simulated individual walkers (Figure 1C,D), the traces with large run-length are found predominantly near the mean velocity, and the traces showing the large deviation from $\overline{V}$ always have a short run-length. The full width at half maximum (FWHM) of Equation 3 is $2(2^{\frac{2}{3}}-1)^{1/2}(\overline{VD}/\overline{L})^{1/2} \approx 3.1(\overline{VD}/\overline{L})^{1/2}$. The predicted velocity distribution is confirmed by simulating the Poisson walkers (see the fit of $P(V)$, red line in Figure 1D, using Equation 3).

2.4 | Single kinesin motors exhibit heterogeneity inside cells

Because initial bead experiments, combined with theoretical analysis, suggested that there was more heterogeneity than expected, we wondered whether such behavior was actually observed in vivo. To test this, we carried out comprehensive tracking and analysis on previously recorded movies of tail-less Kinesin motors (K560) fused to ~24 GFP molecules through the SunTag fluorescence labeling system[26] that had been imaged moving in cells. Importantly, because these are truncated motors lacking their tails, they are unable to bind to cargos, so any differences in motion likely do not reflect differences in what cargos they are attached to. Our analysis involved tracking all detected moving motors, and then eliminating from the dataset those that did not have well defined velocities (ie, we excluded from our analysis those trajectories that involved detectable pauses). We note that this elimination of some runs tends to suppress low-velocity counts, because any run including a pause has a lower average velocity when the pause is included in the calculation of velocity. Although the resultant individual runs were all well behaved, with well-defined average velocities (see Figure 2A, right panel), analysis showed that the resultant velocity histogram (Figure 2B) was left-skewed, and not well described by the distribution of homogeneous ensemble of motors in Equation (3). Instead, the distribution could be fit (see Figure 2B, overall fit curve and sub-population curves) using the functional form developed in the theoretical analysis, reflecting a distribution with 2 subpopulations (see Appendix S1; table with fitting values). This analysis was thus consistent with the hypothesis that there is indeed heterogeneity of function in vivo. In vivo, while such heterogeneity could reflect actual heterogeneity in single-molecule function (eg, due to differential protein folding), it could also result from motion along different classes of microtubules (with different post-translational modifications or different MAPs), or might reflect motors with different post-translational modifications (which altered their velocities).

Clearly, in the experimental conditions the velocity distributions from the kinesin ensemble are asymmetric with respect to the global mean, and their dispersions are greater than those for velocity distributions from homogeneous ensembles. Thus, they should be decomposed into more than a single component. While some of the distributions can in principle be described using a model with more than 2 subpopulations, adding another subpopulation to the model demands 4 extra parameters (V, D, L and ϕ) to be determined, which both excessively complicates model analysis, and does not improve goodness of fit. Thus, to describe the kinesin heterogeneity, we stick to a minimal heterogeneity model with 2 subpopulations, although cannot exclude the possibility that 3 or more subpopulations might be present.

2.5 | Bacterially produced single kinesin motors exhibit heterogeneity in vitro, even without cargos

Because heterogeneity in vivo could be explained via post-translational modifications, we decided to study motors in vitro in a purified well-controlled system. To do so, we make K560-GFP[16] motors in *Escherichia coli*, to avoid post-translational modifications. Importantly, because the motors were fusion proteins, with a GFP tag, we did not need to attach any artificial cargo (polystyrene bead or quantum dot) for visualization to the motors, eliminating concerns that varying cargo attachment geometries could be responsible for any observed heterogeneity. By using a Total Internal Reflection Fluorescence (TIRF) imaging setup, we were able to observe many motors in parallel, allowing collection of significant statistics of single-motor function (see Movie S1). Again, data was filtered to eliminate any questionable tracks with pauses. Typical filtered experimental traces (correlation coefficient > 0.95) and the corresponding velocity distribution are shown in Figure 5 (pH 6.9), respectively. As for the in vivo data, the distribution of velocities could not be well described as a single population, but was reasonably modeled as the sum of

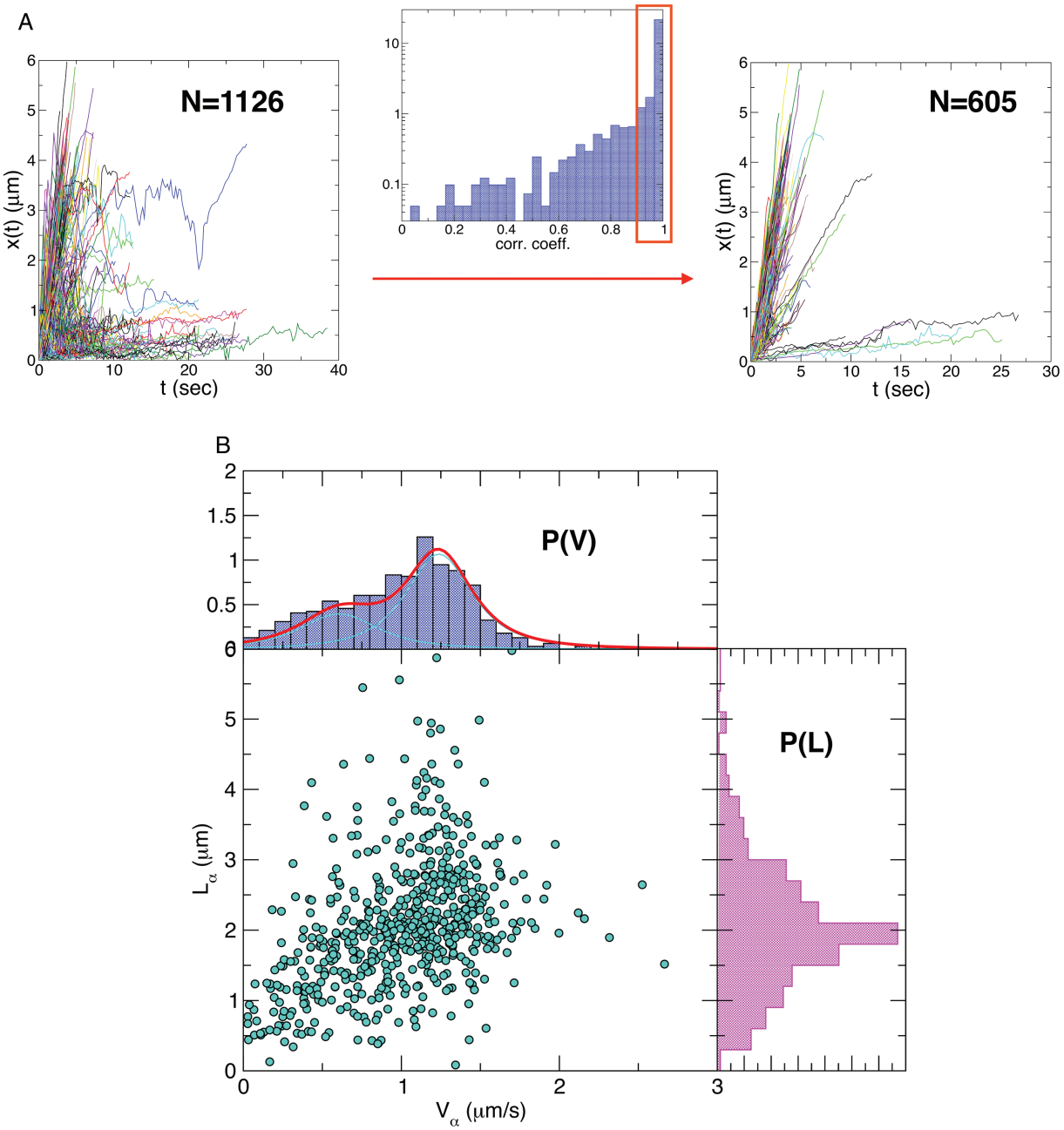

FIGURE 2 Time traces of GFP-tagged K560 moving in mammalian cells (A). Time traces of GFP-tagged K560 (N = 605), which display persistent movement along microtubules inside cells, are filtered from the original set of data (N = 1126), based on the value of correlation coefficient (c.c. > 0:9) for linear regression. B, Scatter plot of the velocity and run-length calculated for the individual motors whose time traces are shown in right panel of (A) (N = 605), including a fit reflecting terms from formula 3 (with 2 velocity populations). Because of measurement uncertainty, extremely short runs were predominantly missed in the analysis

2 distinct populations (see fit lines reflecting individual sub-populations, as well as overall fit line reflecting sum). These in vitro tracks were obtained from motors walking along taxol-stabilized microtubules made from MAP-free tubulin purified from pig brain, polymerized in vitro, and as such all microtubules are expected to be identical, though in principle pre-existing post-translational modifications could have altered MT polymerization. To test this possibility, we looked for isolated microtubules in very long movies, and examined the distribution of k560-gfp velocities along those microtubules. We found multiple examples of variable-velocity motion along the same microtubule, see Figure 3. Thus, the observed heterogeneity seems unlikely to be explained due to variations in MT post-translational modifications.

2.6 | Raised-MT experiments to evaluate potential surface effects

Could velocity heterogeneity reflect variable interactions of the motors with the coverslip surface, where motors moving along protofilaments close to the surface had larger surface interactions which

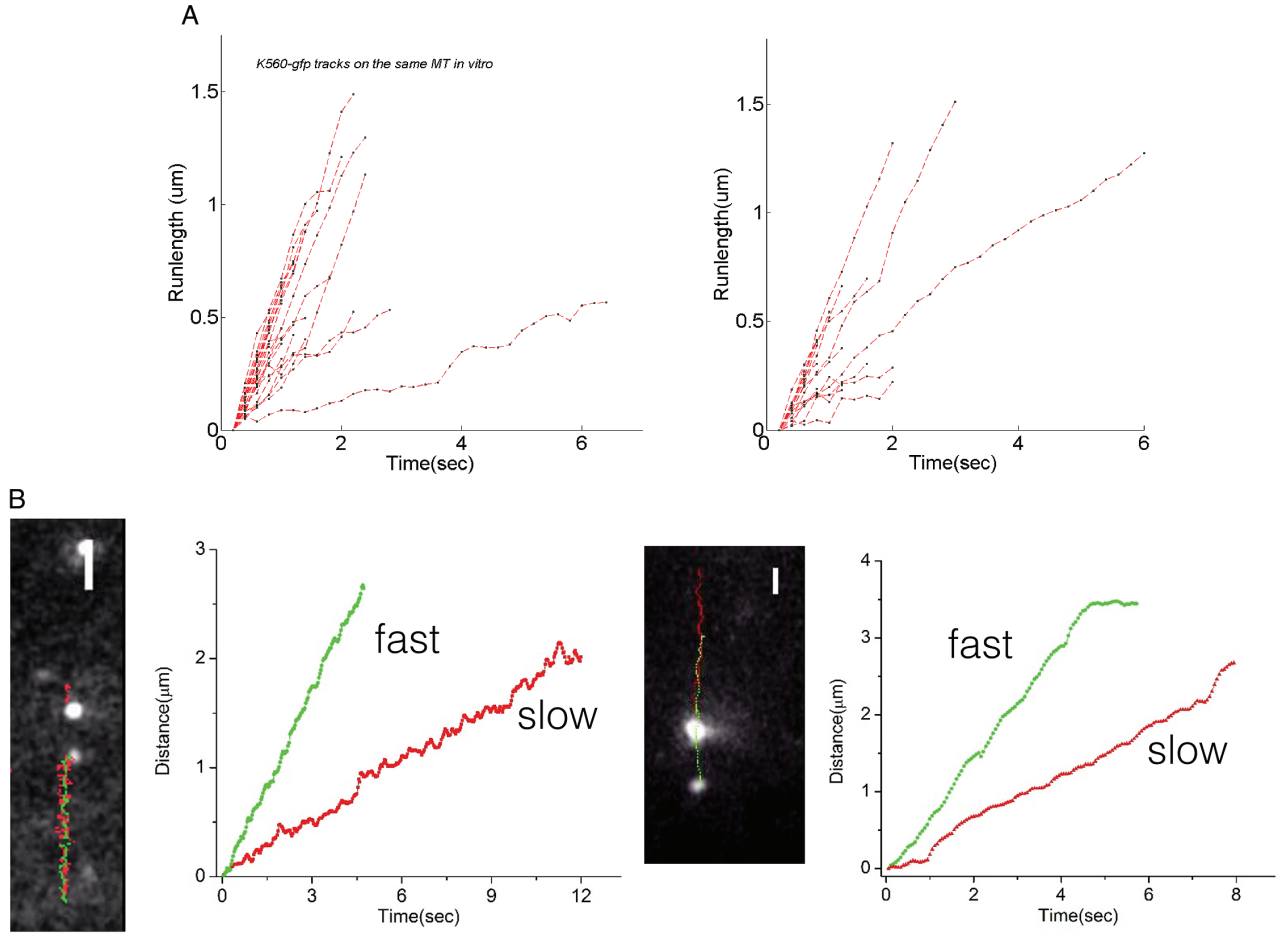

FIGURE 3 Examples of velocity heterogeneity on the same microtubule. (A) examples of multiple single-motor tracks, moving on the same surface-imobilized microtubule, for two independent microtubules. (B) two different examples of different motors moving on two different elevated microtubules. (Overall N = 50). White scale bar in images is 500 nm.

slowed them down and those on protofilaments away from the surface were not so affected? To test this, we developed a new assay to visualize motors moving along levitated microtubules, held away from the surface by attaching them to surface immobilized beads. In this assay, motors were attached via engineered linkages to quantum dots (the GFP tag used for the TIRF setup was not bright enough to be used away from the surface). Then, by using a cylindrical lens setup[27] (Figure S2A) we were able to determine the distance of the motor from the surface by the amount of astigmatism, and then tracked motors moving at least 500 nm from the surface. We still observed heterogeneity (Figure 4), and indeed as for the surface-attached MTs in Figure 3, in some cases observed both a slow and a fast motor moving along the same microtubule, Figure 3. While only a few examples are shown in Figure 3, such cases were not uncommon. It

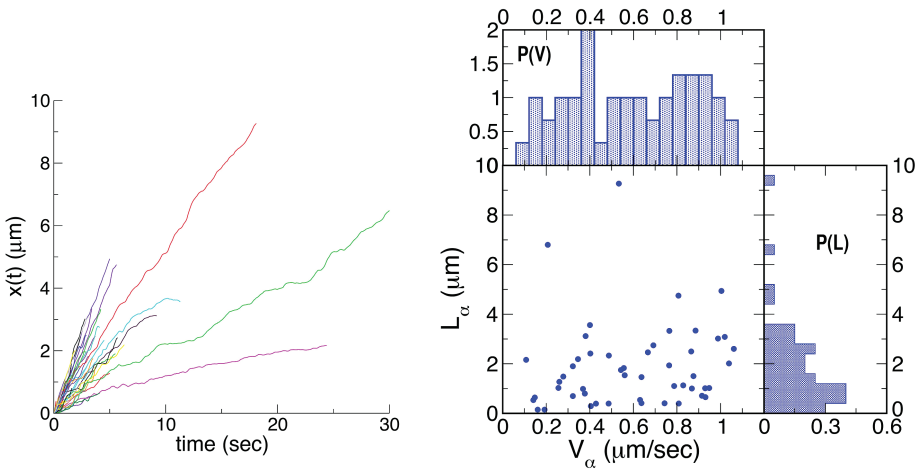

FIGURE 4 Kinesin-560-His_AB-Qdot-655 trajectories on elevated MTs showing heterogeneity in speed(left). Theoretical analysis of the data from left panel showing sub-populations(Right).

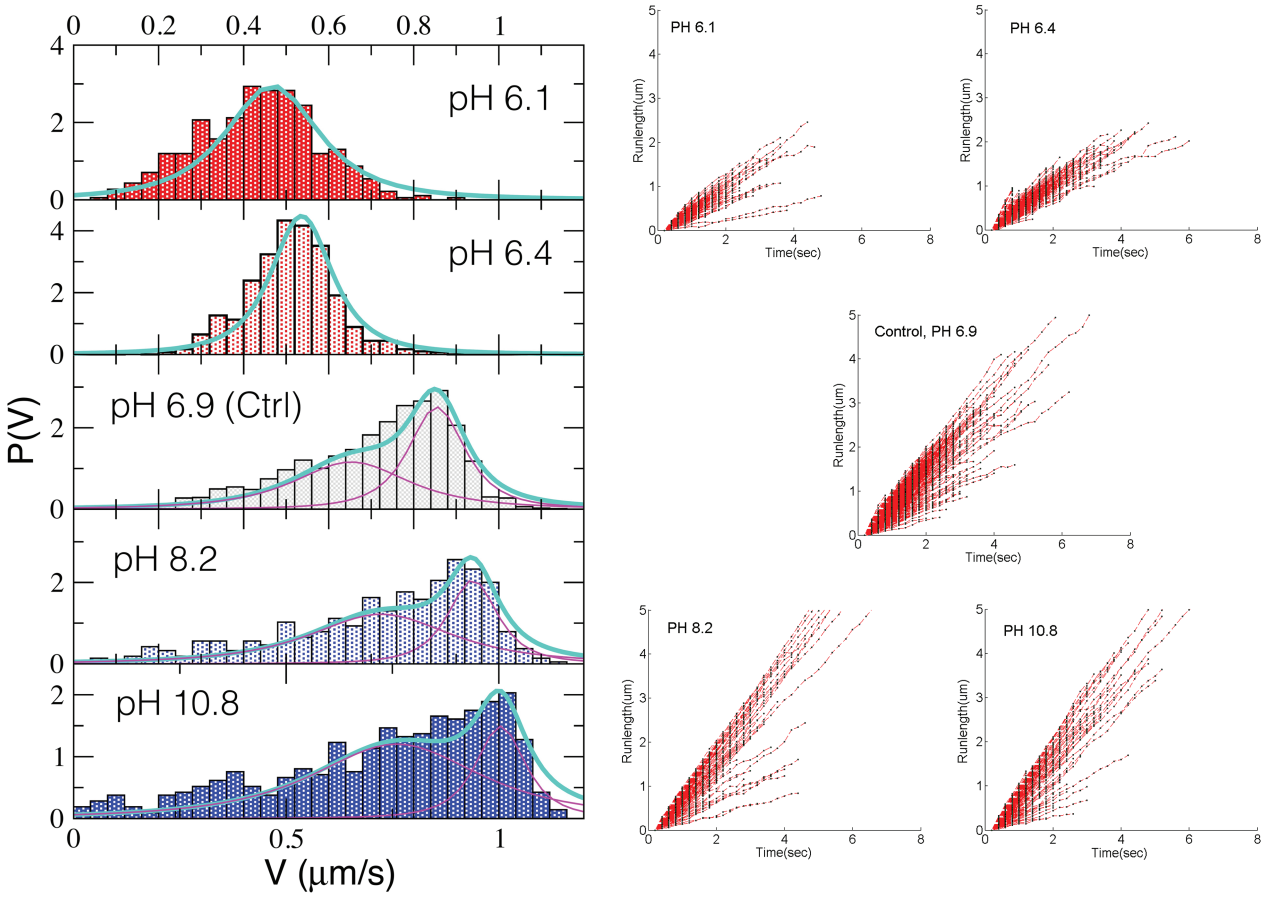

FIGURE 5 Effect of pH on velocity distribution: K-560 velocity distributions obtained from motility experiments with low (6.1 and 6.4) and high (8.2 and 10.8) pH motility buffer, as well as regular (~6.9) pH buffer. Low pH reduced the velocity heterogeneity (top 2 panels). The panels on the right correspond to typical time vs displacement trajectories of k-560-gfps on MTs, with pH as indicated. The run lengths shift towards longer distributions with increasing pH (see Figure S3). In all cases, light blue line indicates composite fit, purple lines indicate sub-population fits

thus seems unlikely that the observed heterogeneity could be explained as entirely due to post-translational modifications, or due to varying surface interactions, although the possibility that microtubule heterogeneity also contributes to functional heterogeneity cannot be excluded (see discussion). Because of this, we next entertained the possibility that the heterogeneity might reflect 2 or more distinctly folded functional states.

2.7 | Use of pH to explore possible differential sensitivity of the 2 sub-groups

Considering that the differential function of the motors might result from the proteins being folded differently, with functional differences in enzymatic activity explained due to slightly different conformations of the enzyme, we decided to test a variety of perturbations typically used to affect protein folding. Our first such perturbation was pH, where we carried out paired sequential experiments in a range of pH conditions, to see if altering pH would change the percentage of motors in slow vs fast states. In addition to testing function at our normal pH of 6.9, we now also looked at motion in lower (pH 6.1 and 6.4) and higher (pH 8.1 and 10.85) pH solutions. We found that the partitioning between slow and fast states was indeed sensitive to pH (Figure 5): at pH 6.9 the fast runs were observed 64% of the time (similar to the 70% observed in cells, see Table S1), whereas at pH 6.1 and 6.4 there was predominantly only a single population (see Appendix S1, for fitting parameters, Supporting Information). Further, in the higher pH backgrounds, the maximum motor velocity increased, but the percentage of runs in the "fast" population was considerably reduced (see fits, Figure 5 and table in Appendix S1). Thus, pH did have a large effect on the relative frequency of slow vs fast motors, consistent with multiple folded states of the kinesin protein, with each folded state having its own sensitivity to changes in pH. The distribution of run-lengths was consistent with single-motor function in all cases (see Figure S3).

2.8 | Use of glycerol to potentially alter protein folding

In addition to changes in pH, protein studies often use glycerol as a "crowding agent" to alter protein folding, and in particular, to stabilize particular stable states without large charges in pH, dielectric constant or changes in the configuration of native protein structures.[28] Glycerol has been shown to assist in proper in vitro folding,[29–31] stabilize folding intermediates[30,32,33] and induce compression of the protein.[32,34] Thus, we tested in paired sequential experiments whether either 15% or 30% glycerol (w/v) would affect the proportion of K560-gfp in slow vs fast states, relative to the wild-type experiments done without additional glycerol. We found that it did (Figure 6A): in

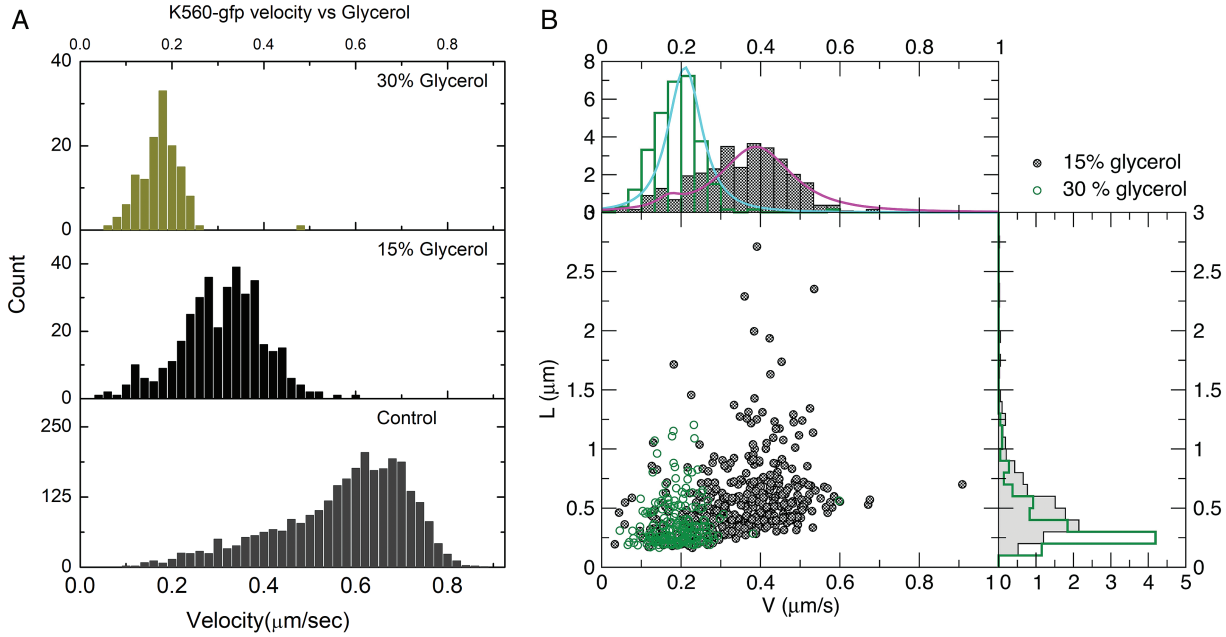

FIGURE 6 Glycerol decreases velocity heterogeneity. (A) In comparison to control (0% glycerol), as increasing amounts of glycerol are added to motility buffer, motors' velocity heterogeneity is reduced. (B) Length-velocity relationship for motors moving in 15 and 30% glycerol.

the 15% glycerol background, ~95% of the runs were in the "fast" subpopulation, although the mean velocity of this subpopulation was decreased, and with 30% glycerol present, the velocity distribution was well modeled by a single population (Figure 6B; table in Appendix S1). Thus, the presence of glycerol did indeed change the relative fraction of slow vs fast motors, consistent with the hypothesis that there are multiple folded functional states of kinesin, some of which are more sensitive to glycerol.

2.9 | Use of temperature to potentially alter protein folding

In a protein folding landscape, one typically envisions one true energy minimum, and then a number of additional local minima with somewhat larger overall energies. Here we are imagining that the kinesins we are studying are trapped in a number of such minima, many of which are functional from the point of view of the motor walking along the microtubule, but each with a slightly different parameters characterizing function; we are using velocity as a simple readout of such functional divergence. A final test of this general notion involves changes in temperatures: if there are indeed multiple functional intermediates in low-energy local minima, the temperature change could repopulate the motor ensemble on the energy landscape, and potentially help motors stuck in local minima to escape, with the result that more motors end up in a true minimum. Thus, we carried out paired TIRF/GFP-K560 single molecule sequential experiments at room temperature, 34 and 37°C. We found that while increasing the temperature lead to a broader spread of velocities, when we did the fitting/partitioning, more of the population was found in the high-velocity state (Figure 6; table Appendix S1). This observed increase in velocity when kinesin-1 functions at higher temperatures is consistent with previous observations.[35] Because temperature changes can alter pH, and above we showed that pH altered function, we checked that in this case, pH change was not significant (~0.2 decrease). In conclusion, the 3 variables we tested known to alter protein folding—pH, glycerol and temperature—all had effects consistent with the hypothesis that K560 may be functioning with multiple different folded states. We note that in each case, relative to the "control" experiment done at the same time, and with the same protein, each of these conditions altered the proportion of motors in the high-velocity state. All such experiments were carried out in at least 3 different independent replicates, on different days. There was typically some variation in the proportion of the wild-type population in the fast state (between 0.5 and 0.65; see table Appendix S1), but the relative changes were consistent and of the same magnitude—that is, for example, the high-temperature data always showed an ~10/20% shift to a higher proportion of high-velocity cases (depending on 34 vs 37°C, respectively), and so on. The distribution of run-lengths was consistent with single-motor function in all cases (see Figure S4).

2.10 | Effects of heterogeneity on multiple-motor function

Regardless of the cause of the heterogeneity, it is important to appropriately characterize it, because one goal of single molecule studies is to measure properties to allow prediction/calculation of ensemble function. Ensembles of heterogeneous molecules might in principle function quite differently from ensembles of homogeneous ones. For instance, heterogeneous motors might interfere more with each other, and in general systems combining multiple motors with different velocities, unexpected ensemble properties can emerge.[36–39] For multiple motors functioning together, past studies found that an overall velocity decrease can lead to a dramatic increase in mean travel distance of a multiple-motor ensemble,[25] suggesting that perhaps a combination of a fast and slow motor might provide an intermediate effect, with somewhat increased mean travel

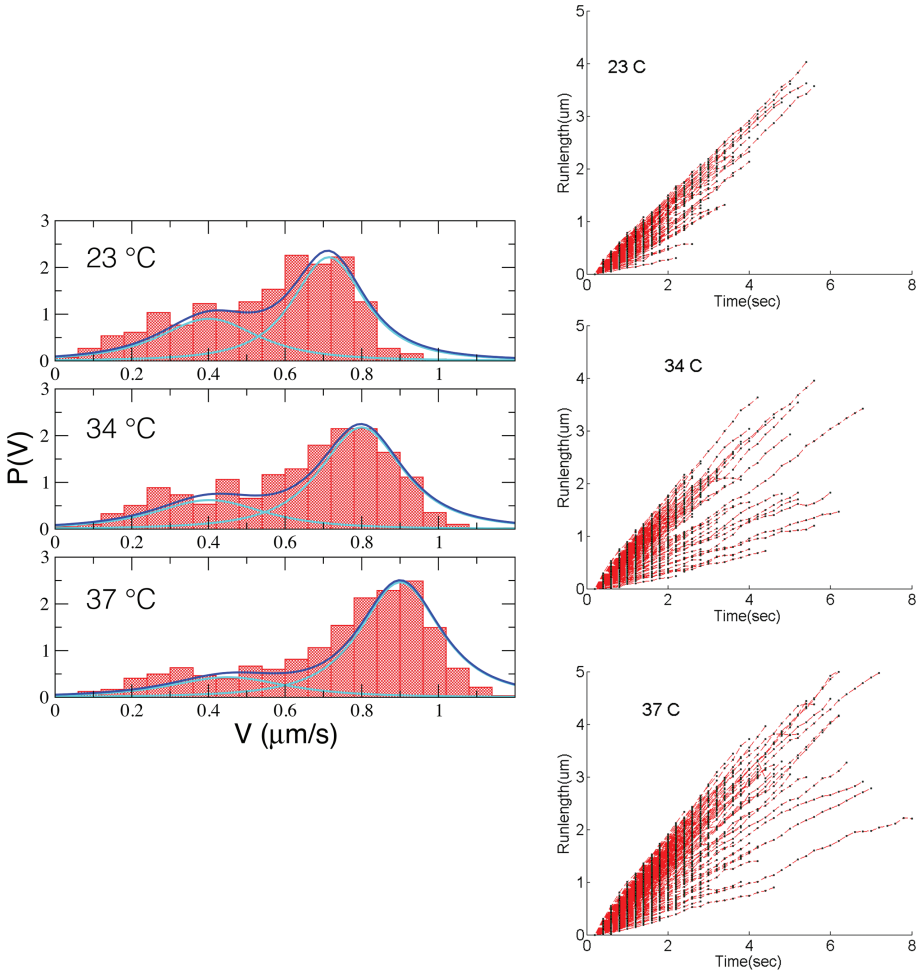

FIGURE 7 Kinesin velocity spread increases with temperature. The distributions correspond to the motility data from experiments at RT, 34°C and 37°C. The panels on the right correspond to typical time vs displacement trajectories of K-560-gfps walking on the MTs. Run length distributions shift towards higher weight with increasing temperature (see Figure S4)

distance. However, a comparison of theoretical predictions[36,40] to experimentally measured two-motor travel distances suggests that motors do not work cooperatively as well as might be expected.[13,41] Although the underlying mechanistic cause of this difference is currently unknown, because the theoretical modeling extrapolates using relatively well-characterized single-molecule properties, the difference suggests some sort of motor-motor interference that could in principle be exacerbated by heterogeneity.

Here, to explore effects of heterogeneity, we use a previously developed Monte-Carlo framework, where 2 motors are attached to a cargo at a point (Figure 8A), and are assumed to interact only through the cargo. Differences in single-motor velocities will likely lead to stress between the motors (with the fast motor in front, pulled back by the slow motor, and vice versa), so we were careful to consider different models for how the motors respond to (directional) load. Importantly, recent work[5] measured kinesin processivity under forward (assisting) as well as backward (opposing) load, and revealed an asymmetric dependence on the direction of load: motors under a forward load exhibit significantly reduced processivity compared with motors under the same magnitude backward (opposing) load. This was implemented, such that the parameters of load-dependent off rates for simulated single motors (Figure 8B) were in accord with experimentally characterized single motor properties. We ultimately compared predicted behavior of a 2-motor system under 2 different models of motor processivity in response to the forward load:

"ε_{nsAL}" model: Off-rate (or detachment probability) insensitive to the forward load (ε_{nsAL});

"ε_{sAL}" model: Experimentally determined off rate dependence (Figure 8A,B) on forward load (ε_{sAL});

Our simulations reveal that, when compared with single motor travels, the 2 motor run distances increase by ~3.1× for ε_{nsAL} model and ~2.3 in ε_{sAL} model (Figure 8C, last bar). The reason that travel enhancement is less in the case of ε_{sAL} is that (Figure S5E) when there are velocity fluctuations and one motor moves more slowly, the slow motor detachment probability increases with assisting load due to the pull from fast motor, whereas it is unaffected in ε_{nsAL} (Figure S5D) (see Appendix S1 for details of how individual and 2-motor groups behave on cargo under the 2 models).

Having implemented these differences, we were then able to look at the effect of intrinsic velocity differences, rather than simply those due to stochastic variation. The larger the velocity difference between the 2 motors, the less cooperative they are (Figure 8C). From this, one might assume that heterogeneity was in fact bad for function, resulting in impaired group function. To test this idea, we imagined a few different pools of heterogeneous motor (distributions shown in Figure 8D), and randomly drew 2-motor pairs from such distributions, and simulated motion (Figure 8E, last three bars). To our surprise, the mean travel of the simulated cargos using the heterogeneous motors was longer (Figure 8F, top) and cargo velocities widely distributed when compared with identical motors (Figure 8F,

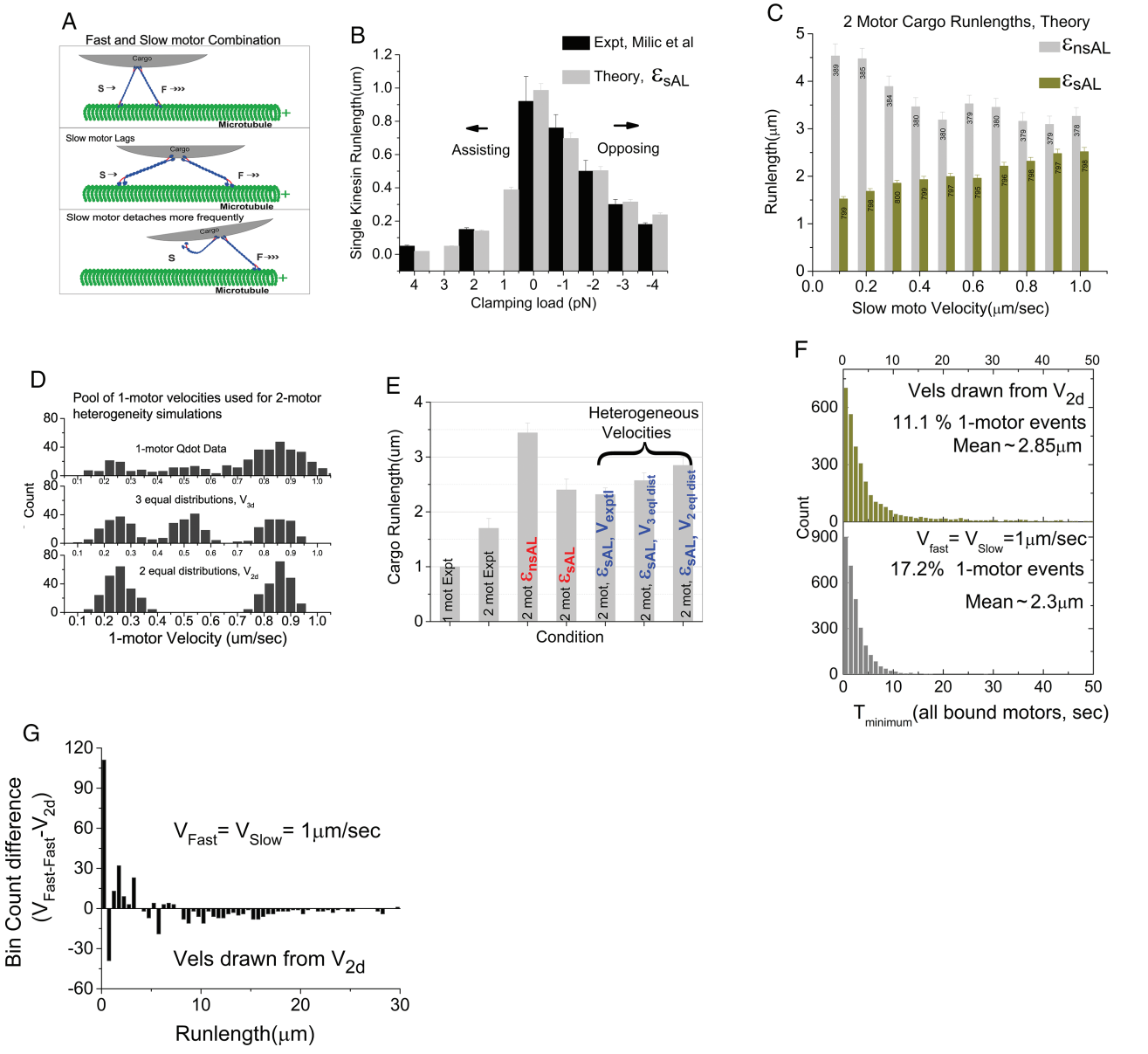

FIGURE 8 A, Schematic illustrating typical functioning of slow and fast motor under model "ε_{sAL}". B, Experimental and simulated single motor cargo run-lengths under constant assisting and opposing applied load. Error bars = SEM. C, Two motor cargo run-lengths for different detachment sensitivities to assisting load "ε_{nsAL}," and "ε_{sAL}." See Figures 8, S1, and S2 for individual motor processivities in the 2-mot group and cargo velocities. Error bars = SEM. (D) Three different *P*(*V*)s used to simulate 2-motor systems. E, Comparison of experimental and simulated mean run-lengths of 1 motor and 2 motor cargos. F, Simulated distribution of times taken for the 2-motor cargos to reach the state of all bound motors. G, Large heterogeneity leads longer runlengths (V_{2d}). Differences in the bin counts for runlength distributions generated using velocities drawn from V_{2d} and V_{fast} = V_{slow} = 1 microns/s

bottom, Figures S5G,H and S6A) although the single-motor travel distances were independent of velocity (Figure S5C).

To better understand this difference, we looked at the difference between the two distributions (Figure 8G). Two features stood out. The first is that in the heterogeneous case, there were more very long runs (bins below the *X*-axis). We believe this results from the occasional random pairing of slow-slow motors, because our past work[13] (and Figure S5A,B) show that decreasing velocities of all motors can significantly enhance multiple motor travel. The second difference was that there was a dramatic suppression of extremely short runs in the heterogeneous case: the first bin is strongly positive. This suppression of very short runs reflects a significant increase in the percentage of the population that makes it to steady state: initially a single motor binds, and if the first motor detaches before the second one binds, the system fails to reach steady state. Heterogeneity frequently involves a slow motor and a fast one. If the slow motor binds first, then because its detachment rate is proportional to its stepping velocity, its temporal detachment rate can be considerably slower than that of the fast motor. Thus, the fast motor has a higher probability of binding before the first (slow) motor detaches, making it more likely for the system to reach steady state. Indeed, the probability of reaching steady state was dramatically different: in the homogenous case, roughly 17% of the events ended before reaching steady state, whereas in the heterogeneous case, only ~11% did (Figure 8F, G).

In conclusion, while velocity differences impair motor-motor coordination because the fast motor causes the slow motor to detach more frequently, for random mixtures of heterogeneous motors, 2 other effects minimize any expected impairment in travel distance, and instead lead to increased travel. The first is the positive effect of slow-slow motors to promote long-distance travel, and the second is the fact that combining slow and fast motors tends to increase the probability of the system reaching equilibrium before the first motor detaches.

3 | DISCUSSION

Here we provide experimental evidence of heterogeneity in in vivo and in vitro molecular motor function, which cannot be explained by stochastic variation in motor stepping times. We provided data showing that[1] kinesins expressed from different organisms (*Drosophila*, Mammalian cells, *E. coli*) display functional heterogeneity in velocity (Figures 1 and 5) and that this heterogeneity probably occurs in vivo because it is also seen in single kinesins expressed in cells (Figure 2). The live cell and Q-dot data from elevated MTs show that the heterogeneity exists even in the absence of a surface effect (Figures 2–4, Figure S2 and Movie S2). Further, multiple observations of slow and fast moving motors on the same MT (Figure 3) argue against the heterogeneity arising solely from altered tubulins (see also Movies S3–S5). The additional experiments carried out using GFP tagged K560 confirm the presence of heterogeneity in translocation rates and rule out any possible interference due to details of cargo attachment. The relative frequency of the different functional states could be altered by pH, glycerol and temperature variation. Addition of 30% glycerol eliminated velocity heterogeneity, potentially by forcing the kinesins into single folded state, while at 15% glycerol in the buffer the velocity distributions point to the presence of only a very small amount of a second population (Figure 6). Overall, our results are thus consistent with the hypothesis of the existence of multiple functional folded states of kinesin, because various protein folding studies suggest that glycerol aides better protein folding,[28–30,34] and pH and temperature also are known to alter protein folding. While we favor this model of multiple folded functional kinesin states, we cannot exclude the possibility that some of the observed functional heterogeneity results from microtubule heterogeneity. In principle, the post-translational modifications of the tubulin could affect in vitro polymerization, so that our "identical" microtubules might not be. Nonetheless, 2 observations suggest the functional heterogeneity is unlikely to be explained solely due to MT post-translational modifications. First, there are numerous independent examples of slow and fast motors moving on the same microtubule (see eg, Figure 3). Second, while pH might affect the motor-tubulin-c-terminal tail interaction, neither temperature nor glycerol should alter the presence of c-terminal post-translational modifications, but they do alter the motors' velocity heterogeneity.

In summary, because we observed kinesins which travel with persistently different mean velocities on the same MT (Figure 3, Movies S2 to S5), and the frequency of velocity groups can be affected by glycerol and temperature as well as pH, we believe that the functional heterogeneity is intrinsic to the motors themselves, not caused by the heterogeneity in MTs or roadblocks on them.[42] Instead, single motors appear to have relatively well defined—but different—mean stepping rates. As we characterize single-motor function, we cannot determine whether this functional heterogeneity occurs because of differences between the motors' heads, or some variation in folding in the motors' stalk. However, this functional difference is reminiscent of the dynamical heterogeneity observed in the movement of a more complicated molecular construct RecBCD.[22] While such functional heterogeneity is also seen for single kinesin molecules functioning inside of cells and cell lysates[9] for the in vivo case, it was unclear whether the observed heterogeneity was due to single-molecule heterogeneity, or rather, to unknown cofactors/post-translational modifications affecting motor function, combined with microtubules with different properties due to maps, post-translational modifications, and so on. The in vitro effects likely do not result from such mechanisms, suggesting that perhaps the observed in vivo heterogeneity is also due in part to single-molecule heterogeneity. At the very least, it suggests additional in vivo experiments should be done to test the previously unquestioned assumption that any variation in function in vivo is likely explained by post-translational modifications.

In vivo, cargos are frequently driven by more than one motor,[19,43–45] so we characterized effects of heterogeneity on group function. We found that the motors' detachment kinetics, especially under forward (assisting) load, matter significantly; this was consistent with a recent study examining motility driven by teams of a mixed family of kinesin motors.[10,12,46] If the motor detachment kinetics are insensitive to forward load, slower motors decrease the overall ensemble velocity of 2-motor cargos, while increasing overall average cargo travel distances (Figure 8C). If the single motor detachment kinetics are sensitive to forward load—experimentally the case for kinesin-1—then the slow motor will not slow down the cargo, but instead detaches rapidly. Then, for cargos with 2 such heterogeneous motors, mean velocity is unaffected, but mean cargo travel distances are reduced relative to 2 homogeneous motors. However, when we randomly choose motors from a highly heterogeneous population, decreased travel distances due to a slow-fast pairings are countered by longer travels from slow-slow pairings, and by an increased likelihood of avoiding premature detachment, so the effect of the heterogeneity on mean travel distance is moderately positive. Interestingly, for identical (non-heterogeneous) motors, motor-motor interference increases with increasing numbers of motors in the ensemble (Figure S6B): the decrease in single motor processivity when the motor is in a group of 2 is only ~18%, but is almost 50% when functioning in a group of 5 (this latter result is consistent with others simulations on larger groups of kinesins[12]).

In our simulations of 2-kinesin motor cargos expected to approximate experiments (ie, velocities of the simulated motors drawn from the experimentally observed $P(V)$, and with single-motor's off-rate sensitivity to forward load ("ε_{sAL}"), we found that the 2 motor enhancement of travel was ~2.4×, significantly larger than the experimentally observed enhancement of ~1.7× observed by us[13] and others.[9,41] Thus, it does not appear that a combination of

heterogeneity with motor-motor interactions through the cargo are sufficient to explain why the experimentally observed enhancement is so low. Assuming the simulations correctly capture motor-motor interactions due to internally generated strain, what is left as the only "free parameter" is the dependent on-rate, that is the on-rate of the second motor when the first is already bound. To account for the low (1.7) enhancement, we thus hypothesize that the second motor's on-rate is decreased when the first is bound. This hypothesis remains for future experiments to test.

In summary, for Kinesin-1, evolution appears to have selected for maintaining group velocity at the cost of only slightly increasing run-lengths; if motors were insensitive to forward load, run-lengths would be more significantly enhanced.

Our study did highlight an advantage of heterogeneity: we find the unexpected result that the heterogeneity roughly halves the number of runs that do not reach the steady state; this could be important in cases where the overall number of moving cargos matters: if microtubules are relatively sparse, when a cargo detaches from the microtubule, it could diffuse away and subsequently remain unmoving in the cytosol for a considerable amount of time before eventually reaching a new microtubule.

More generally, examples of heterogeneity in single-protein function are increasing, and may hold true for more complex biological machines, like ribosomes, as well, as translation elongation speed also shows substantial heterogeneity for different ribosomes.[47] Although the importance of heterogeneity is increasingly appreciated at the cellular level,[48,49] it is still surprising to observe such characteristics at the level of single biomolecules. The structural origin of functional heterogeneity potentially reflecting multiple native states[22,23] is not clear. Yet, our data is consistent with the hypothesis that kinesin can indeed have multiple functional states with distinct ATP processing capability, which gives rise to fast and intermediate/slow groups of motors. Because the conformational cycle of kinesin is driven by chemical potential from ATP hydrolysis, functional states of motile kinesins are perhaps dynamically pinned, or separated by large free energy barrier over which no thermodynamic path can easily connect one state with another. Although it is not easy to test this hypothesis for kinesins due to their short processivity, recent studies of Holliday junctions[21] and RecBCD[22] have shown that subensemble-to-subensemble interconversion can be induced by depleting cofactors (Mg2+ and ATP, respectively) for a finite amount of time.

In summary, we provide quantitative criteria to determine when experimentally observed heterogeneity is too large, that it cannot be due simply to stochastic variation, suggest that such heterogeneity may result from slightly different alternative folding geometries, and explore ramifications of such differences in function at the ensemble level. While evolution appears to have chosen detachment kinetics which minimize the effect of velocity heterogeneity on ensemble velocity, heterogeneity does increase the probability of the cargo reaching steady-state motion; the overall utility of such effects, and heterogeneity more generally, remains to be explored. One appealing notion is that having multiple functional states with different properties already present allows evolution to more rapidly act to develop new functional variants, via mutations that selectively bias folding towards a particularly useful functional state. It remains for future work to explore such possibilities.

4 | MATERIALS AND METHODS

4.1 | Protein purification

Purification of Drosophila full-length kinesin is as explained in Reference 15. To ensure that the population of kinesins are chemically "identical", we expressed the functional, truncated kinesin (K560) and K-560gfp in *E. coli* and purified it as reported earlier.[8,16,50] The procedure briefly is, *E. coli* Rosetta cells were transformed, and grown at 37°C from a single colony in 500 mL of terrific broth. Once a cell density between OD 600 1.5-2 was reached, expression was induced with 2 mM IPTG at 18°C for 48 h. Cells were pelleted at 5000 rcf for 10 minutes at 4°C, and resuspended in Kinesin Wash Buffer (50 mM sodium phosphate, pH 7.4, 300 mM NaCl, and 75 mM Immidazole). Resuspended cells were lysed by sonication and cell debris was pelleted by a 25 000 rcf spin for 60 minutes at 4°C. The lysates were then filtered (0.22 um). K560-His was then bound to Ni^{2+} affinity column (Ni-NTA-resin Qiagen, Inc.) via 1 hour incubation with the lysates at 4°C with light agitation. K560-His was eluted with Kinesin Elution Buffer (same as Kinesin Wash Buffer, but contains 250 mM Imidazole). Glycerol was added to final concentration of 10% to the eluted K560-His, and this was snap frozen and stored at −80°C. Note that the lack of light chains (tails) prevents potential interactions between light and heavy chains that may alter function. Further, we minimized the chance of phosphorylation, another potential source of chemical heterogeneity, by expressing the kinesins in *E. coli*. Furthermore, to select only the functional kinesins, the stock protein was selectively purified via MT binding and release in the presence of AMP-PNP (the non-hydrolysable ATP analogue).[4] Reported experiments were carried out using multiple independent purifications of kinesin.

4.2 | Motility experiments

Single motor bead experiments with kinesin were carried out using the methods reported earlier.[15,51] For all the motility experiments, freshly thawed kinesin motors taken out from −80°C freezer were used. Each thawed aliquot was used only once and a new aliquot was thawed each time when the measurements were repeated or for the next set of experiments. The particle tracking and analyses was carried out on the movies captured within ~30 minutes after thawing.

4.3 | K560-24xgfp expression in cells

U2OS cells were grown in DMEM supplemented with 10% fetal calf serum (FCS) and Pen/Strep, and were transfected with Fugene 6 - (Roche). Cells were imaged 24 hours after transfection. For time-lapse microscopy, cells were grown in 96-well glass bottom dishes (Matriplate, Brooks) in DMEM:F12 (1:1) medium without phenol red, supplemented with 20 mM HEPES to maintain a correct pH independently of CO_2. During imaging, cells were maintained at 37°C in a temperature-controlled chamber. Cells were imaged using an inverted

Nikon TI spinning disk confocal microscope with the Nikon Perfect Focus system, a 100× 1.45 NA objective, an Andor 897 EM-CCD camera, and Micro-Manager software.[52] For single molecule imaging of K560-SunTag, 2x2 pixel binning was applied, resulting in a pixel size of 166 nm. Movies were acquired under continuous illumination for 30 seconds with 0.2 second integration time per image.

4.4 | Specific recruitment of K-560 to Qdots

For the elevated MT assay, K-560-His was specifically recruited to quantum dots via its genetically encoded C-terminal His-tag. To achieve the specific linking of kinesin to the cargo, streptavidin quantum dots (QD-655-streptavidin conjugate, Life Technologies) were labeled with biotin conjugated Penta-His antibody (Qiagen) in molar ratio of 1:1::AB:QD. The incubation temperature of antibody with QDs was 4C and lasted for 1 hour. The AB labeled QD surface was blocked with 4 mg/mL casein (Sigma-Aldrich, C8654-500G) in the motility buffer (80 mM Pipes pH 6.9, 50 mM CH_3CO_2K, 4 mM $MgSO_4$, 1 mM DTT, 1 mM EGTA, 10 μM taxol, 4 mg/mL casein) for 1 hour at 4°C to reduce nonspecific binding. With this blocking procedure K560 binding to casein-coated streptavidin QDs alone (without antibody) was negligible (reduced by 50 times) compared with the same for AB coated QDs. K560 with His tag on its truncated tail was incubated with anti-His antibody tagged QDs in the molar ratio of 1:40 at RT for 12 minutes. Before using the mixture to test motility it was supplemented with 2 mM ATP and oxygen-scavenging system. The high ratio of K560: QD (1:40) was chosen to ensure high probability of recruiting a single kinesin to the QDs.

4.5 | Elevated microtubules

Elevated MTs were constructed by attaching mutant-Kinesin (Serves as anchor; binds to the MTs well but does not translocate in the presence of ATP) coated carboxyl beads (Polysciences, 2% solution, 800 nm polystyrene) to the polylysine coated coverslip. Density of beads in the buffer was optimized to give an average spacing of about 10 μm. About 3 μL of Beads/10 in 30 μL of buffer gave an average spacing of 10 μm between the beads. The beads were incubated for 10 minutes to let them attach to the surface. Next, the surface was blocked with 5 mg/mL casein buffer for 5 minutes at RT to avoid the MTs from sticking to the polylysine-coated surface. As a final step, about 30 μL of taxol stabilized MTs (1/100 dilution, preformed from 5 mg/mL tubulin using 1 mM GTP, 20 μM Paclitaxel, 80 mM Pipes and 5% glycerol, at 37°C for 18 minutes) were flown and incubated for 15 minutes at RT before washing the unbound MTs with motility buffer.

4.6 | TIRF imaging and particle tracking

A sample chamber assembled with taxol stabilized microtubules (elevated or attached to the surface) made from bovine brain tubulin (Prof. Les Wilson's lab) was used for motility experiments. The sample was excited with 488 nm laser (Ti:Sapphire, Coherent) and imaged via a custom TIRF microscope (Nikon 1.49NA, ×100), using EMCCD camera (Photometrics, QuantEM 512SC). All TIRF imaging assays utilized the same motility buffer and flow chamber as for bead assays unless specified otherwise.

The image analysis was carried out using an automated tracking algorithm written in MATLAB (Gross Lab code). The program identifies the positions of the particles via 2-dimensional Gaussian fitting to the point spread function of the fluorescent spots and generates the trajectories of the linearly moving particles.

4.7 | Motility with altered pH, glycerol and temperature

pH of the buffer was altered by adding small volumes (~0.1%) of 1 M HCl and NaOH to the motility buffers supplemented with ATP and oxygen scavengers, just before imaging.

For experiments with changing glycerol, the freshly thawed K560-gfp motors were suspended in the glycerol supplemented motility buffer (15% and 30% w/v glycerol) just before introducing them into flow chamber for measurements.

High temperature measurements were carried out by using a custom built heating stage that maintained the desired temperature within ±1°C during the experiment.

4.8 | Simulation of 2-motor systems

We started with a single-motor model for kinesin, displaying Michaelis-Menten kinetics, following the work of Reference 53. While related to Reference 53 and our subsequent Monte-Carlo model of kinesin previously presented in Reference 54, this new single motor model is an extension: it describes appropriate detachment kinetics when the motor is under super-stall (a force larger than it can move against) as experimentally measured.[54] Further, based on recent work (References 5,53 and M. Lang, personal communication), it assumes that a forward load does not affect kinesins velocity, but does decrease its processivity similar to the effect of a backward directed force of the same magnitude. Complete details of our single-motor model are described in Reference 51.

Briefly, we used the following theoretical relations. Sub-linear force-velocity dependence[51,54]; for leading motor and velocity of lagging motor was assumed to be independent of assisting load.

$$v(F) = v\left(1 - (F/F_s)^W\right)$$

Load dependent motor stepping rates and detachment kinetics were set as reported earlier[51,55]; forward stepping rate, $k_{\rightarrow \text{step}}(F) = \begin{cases} \left(\frac{v}{d}\right)\left(1 - \left(\frac{F}{F_s}\right)^W\right) & F \le F_s \\ 0 & F > F_s \end{cases}$

Exponential detachment kinetics below stall[36]

$$\varepsilon(F) \propto \varepsilon \exp(F/F_d)$$

Advancement of the moving cargo inside the trap between any time interval t and $t + \Delta t$ is $\vec{x}(t+\Delta t) = \vec{x}(t) + \vec{x}_{\text{random}} + \frac{\vec{f}}{6\pi\eta r}(\Delta t)$

Force on the cargo due to multiple dynein motors was calculated as

$$\vec{f} = \sum_{j=1}^{N} k_{mot} \Delta l_j + C_{load}$$

In the above equations, F is the force on the motor head, F_s is the stall force of the motor (1.5 pN), F_d is the detachment force (3.5 pN), C_{load} is the clamping load (assisting/opposing), v is the velocity of the motor(100–1000 nm/s), d-step size of the motor (8 nm), k_{mot} is the stiffness of the motor (0.32 pN/nm), Δl_j is extension of the walking motor j beyond its rest length l (50 nm), r is the radius of the cargo (250 nm), $\vec{x}_{random}$ is the Brownian displacement, Δt is the time step, η − 2 × Viscosity of water, $\Delta t = 10^{-6}$ seconds and $w = 2$, ε = 0.85 second^{-1} and on-rate = 5 second^{-1}.

4.9 | Other simulation parameters

Below are the specific additional parameters that are most likely tuned in the simulation after fixing the values of rest as above.

Figure 8B:

ε_{sAL}: C_{load} = −4 to +4 pN, v_{motor} = 1000 nm/s, $\varepsilon(F) = \varepsilon \times \exp(1.25 \times F/F_d)$,

Figure 8C and Figure S5F:

ε_{sAL}: C_{load} = 0 pN, v_{slow} = 100–1000 nm/s, v_{fast} = 1000 nm/s,

$\varepsilon(F) = \varepsilon \times \exp(1.25 \times F/F_d)$, $\varepsilon(B) = 0{:}92 \times \varepsilon \times \exp(4\ F/F_d)$, N = 500.

ε_{nsAL}: C_{load} = 0 pN, v_{slow} = 100–1000 nm/s, v_{fast} = 1000 nm/s,

$\varepsilon(F) = \varepsilon \times \exp(1.25{*}F/F_d)$, $\varepsilon(B) = \varepsilon$, N = 500.

Figures 8D and G:

To test effect of extreme velocity heterogeneity on the 2-motor cargo travel, different distributions of single motor velocity were selected. 8D, Top Panel: Single motor velocities drawn from the K-560 quantum dot experiment. 8D, Middle & bottom panels: Three and two velocity distributions of equal weight generated by the computer using Gaussian random number generator. The peak centers for V_{2d} are 0.25 and 0.85 μm. For V_{3d} they are at 0.25, 0.51 and 0.85 μm. The centers were chosen based on the Gaussian peaks found in experimental velocities.

Figure S5A:

ε_{sAL}: C_{load} = 0 pN, v_{slow} = $v_{fast=}$ 100–1000 nm/s,

$\varepsilon(F) = \varepsilon \exp(1.25 \times F/F_d)$,

$\varepsilon(B) = 0{:}92 \times \varepsilon \times \exp(4F/F_d)$, N = 400.

Figure S5B:

ε_{sAL}: C_{load} = 0 pN, v_{slow} = 100 nm/s, v_{fast} = 1000-100 nm/s,

$\varepsilon(F) = \varepsilon \exp(1.25 \times F/F_d)$,

$\varepsilon(B) = 0{:}92 \times \varepsilon \times \exp(4F/F_d)$, N = 400.

Figure S5C:

ε_{sAL}: C_{load} = 0 pN, v_{motor} = 100–1000 nm/s,

$\varepsilon(F) = \varepsilon \exp(1.25 \times F/F_d)$,

$\varepsilon(B) = 0{:}92 \times \varepsilon \times \exp(4F/F_d)$, N = 500.

Figure S5D:

ε_{nsAL}: C_{load} = 0 pN, v_{slow} = 100-1000 nm/s, v_{fast} = 1000 nm/s, $\varepsilon(F) = \varepsilon \times \exp(1.25 \times F/F_d)$, $\varepsilon(B) = \varepsilon$, N = 400.

Figure S5E:

ε_{sAL}: C_{load} = 0 pN, v_{slow} = 100-1000 nm/s, v_{fast} = 1000 nm/s,

$\varepsilon(F) = \varepsilon \times \exp(1.25{*}F/F_d)$,

$\varepsilon(B) = 0{:}92 \times \varepsilon \times \exp(4F/F_d)$, N = 400.

Figure S5F: *same as Figure S8C*

Figure S5G:

ε_{sAL}: C_{load} = 0 pN, N = 400.

v_{slow} and v_{fast} chosen from table of velocities obtained in single motor experiment.

Figure S6A:

ε_{sAL}: C_{load} = 0 pN, $\varepsilon(F) = \varepsilon \exp(1.25 \times F/F_d)$,

$\varepsilon(B) = 0{:}92 \times \varepsilon \times \exp(4F/F_d)$, N = 3600.

For top panel, v_{slow} and v_{fast}, chosen from table of velocities in $V_{2d.}$

For bottom panel $V_{fast} = V_{slow}$ = 1 μm/s.

Figure S6B:

ε_{sAL}: C_{load} = 0 pN, v_{motor} = 1000 nm/s,

$\varepsilon(F) = \varepsilon \exp(1.25 \times F/F_d)$,

$\varepsilon(B) = 0{:}92 \times \varepsilon \times \exp(4F/F_d)$, N = 200.

Simulations for 3-, 4-, and 5-motor groups were terminated at t = 20 s to save the computation time.

ACKNOWLEDGMENTS

C.H. thanks Anatoly Kolomeisky and Joe Howard for critical feedback on this work. S.P.G. was supported by NIH RO1 GM123068. Authors acknowledge Dr Siavash Ahrar, Physics Department, UC Irvine for the helpful technical and scientific discussions.

Conflict of interests

The authors declare no conflict of interests.

Editorial Process File

The Editorial Process File is available in the online version of this article.

REFERENCES

1. Vale RD. The molecular motor toolbox for intracellular transport. *Cell*. 2003;112(4):467-480.
2. Vershinin M, Carter BC, Razafsky DS, King SJ, Gross SP. Multiple-motor based transport and its regulation by Tau. *Proc Natl Acad Sci USA*. 2007;104(1):87-92.
3. Shojania Feizabadi M, Janakaloti Narayanareddy BR, Vadpey O, et al. Microtubule C-terminal tails can change characteristics of motor force production. *Traffic*. 2015;16(10):1075-1087.
4. Valentine MT, Fordyce PM, Krzysiak TC, Gilbert SP, Block SM. Individual dimers of the mitotic kinesin motor Eg5 step processively and support substantial loads in vitro. *Nat Cell Biol*. 2006;8(5):470-476.
5. Milic B, Andreasson JO, Hancock WO, Block SM. Kinesin processivity is gated by phosphate release. *Proc Natl Acad Sci USA*. 2014;111(39):14136-14140.
6. Okamoto N, Miya F, Tsunoda T, et al. KIF1A mutation in a patient with progressive neurodegeneration. *J Hum Genet*. 2014;59(11):639-641.
7. Reid E, Kloos M, Ashley-Koch A, et al. A kinesin heavy chain (KIF5A) mutation in hereditary spastic paraplegia (SPG10). *Am J Hum Genet*. 2002;71(5):1189-1194.
8. Xu J, Reddy BJ, Anand P, et al. Casein kinase 2 reverses tail-independent inactivation of kinesin-1. *Nat Commun*. 2012;3:754.
9. Norris SR, Soppina V, Dizaji AS, et al. A method for multiprotein assembly in cells reveals independent action of kinesins in complex. *J Cell Biol*. 2014;207(3):393-406.

10. Jamison DK, Driver JW, Rogers AR, Constantinou PE, Diehl MR. Two kinesins transport cargo primarily via the action of one motor: implications for intracellular transport. *Biophys J*. 2010;99(9):2967-2977.
11. Pan X, Ou G, Civelekoglu-Scholey G, et al. Mechanism of transport of IFT particles in *C. elegans* cilia by the concerted action of kinesin-II and OSM-3 motors. *J Cell Biol*. 2006;174(7):1035-1045.
12. Arpag G, Shastry S, Hancock WO, Tuzel E. Transport by populations of fast and slow kinesins uncovers novel family-dependent motor characteristics important for in vivo function. *Biophys J*. 2014;107(8):1896-1904.
13. Xu J, Shu Z, King SJ, Gross SP. Tuning multiple motor travel via single motor velocity. *Traffic*. 2012;13(9):1198-1205.
14. Larson AG, Landahl EC, Rice SE. Mechanism of cooperative behaviour in systems of slow and fast molecular motors. *Phys Chem Chem Phys*. 2009;11(24):4890-4898.
15. Sigua R, Tripathy S, Anand P, Gross SP. Isolation and purification of kinesin from Drosophila embryos. *J Vis Exp*. 2012;62:3501. https:\\doi.org\10.3791/3501
16. Case RB, Pierce DW, Hom-Booher N, Hart CL, Vale RD. The directional preference of kinesin motors is specified by an element outside of the motor catalytic domain. *Cell*. 1997;90(5):959-966.
17. Visscher K, Schnitzer MJ, Block SM. Single kinesin molecules studied with a molecular force clamp. *Nature*. 1999;400(6740):184-189.
18. Zhuang X, Kim H, Pereira MJ, Babcock HP, Walter NG, Chu S. Correlating structural dynamics and function in single ribozyme molecules. *Science*. 2002;296(5572):1473-1476.
19. Shubeita GT, Tran SL, Xu J, et al. Consequences of motor copy number on the intracellular transport of kinesin-1-driven lipid droplets. *Cell*. 2008;135(6):1098-1107.
20. Lu HP, Xun L, Xie XS. Single-molecule enzymatic dynamics. *Science*. 1998;282(5395):1877-1882.
21. Hyeon C, Lee J, Yoon J, Hohng S, Thirumalai D. Hidden complexity in the isomerization dynamics of Holliday junctions. *Nat Chem*. 2012;4(11):907-914.
22. Liu B, Baskin RJ, Kowalczykowski SC. DNA unwinding heterogeneity by RecBCD results from static molecules able to equilibrate. *Nature*. 2013;500(7463):482-485.
23. Solomatin SV, Greenfeld M, Chu S, Herschlag D. Multiple native states reveal persistent ruggedness of an RNA folding landscape. *Nature*. 2010;463(7281):681-684.
24. Hinczewski M, Hyeon C, Thirumalai D. Directly measuring single-molecule heterogeneity using force spectroscopy. *Proc Natl Acad Sci USA*. 2016;113(27):E3852-E3861.
25. Hyeon C, Hinczewski M, Thirumalai D. Evidence of disorder in biological molecules from single molecule pulling experiments. *Phys Rev Lett*. 2014;112(13):138101.
26. Tanenbaum ME, Gilbert LA, Qi LS, Weissman JS, Vale RD. A protein-tagging system for signal amplification in gene expression and fluorescence imaging. *Cell*. 2014;159(3):635-646.
27. Huang B, Wang W, Bates M, Zhuang X. Three-dimensional super-resolution imaging by stochastic optical reconstruction microscopy. *Science*. 2008;319(5864):810-813.
28. Gonnelli M, Strambini GB. Glycerol effects on protein flexibility: a tryptophan phosphorescence study. *Biophys J*. 1993;65(1):131-137.
29. Gekko K, Timasheff SN. Thermodynamic and kinetic examination of protein stabilization by glycerol. *Biochemistry*. 1981;20(16):4677-4686.
30. Sato S, Ward CL, Krouse ME, Wine JJ, Kopito RR. Glycerol reverses the misfolding phenotype of the most common cystic fibrosis mutation. *J Biol Chem*. 1996;271(2):635-638.
31. Vagenende V, Yap MG, Trout BL. Mechanisms of protein stabilization and prevention of protein aggregation by glycerol. *Biochemistry*. 2009;48(46):11084-11096.
32. Knubovets T, Osterhout JJ, Connolly PJ, Klibanov AM. Structure, thermostability, and conformational flexibility of hen egg-white lysozyme dissolved in glycerol. *Proc Natl Acad Sci USA*. 1999;96(4):1262-1267.
33. Mishra R, Bhat R, Seckler R. Chemical chaperone-mediated protein folding: stabilization of P22 tailspike folding intermediates by glycerol. *Biol Chem*. 2007;388(8):797-804.
34. Priev A, Almagor A, Yedgar S, Gavish B. Glycerol decreases the volume and compressibility of protein interior. *Biochemistry*. 1996;35(7):2061-2066.
35. Nara I, Ishiwata S. Processivity of kinesin motility is enhanced on increasing temperature. *Biophysics (Nagoya-shi)*. 2006;2:13-21.
36. Klumpp S, Lipowsky R. Cooperative cargo transport by several molecular motors. *Proc Natl Acad Sci USA*. 2005;102(48):17284-17289.
37. Gross SP, Vershinin M, Shubeita GT. Cargo transport: two motors are sometimes better than one. *Curr Biol*. 2007;17(12):R478-R486.
38. Soppina V, Rai AK, Ramaiya AJ, Barak P, Mallik R. Tug-of-war between dissimilar teams of microtubule motors regulates transport and fission of endosomes. *Proc Natl Acad Sci USA*. 2009;106(46):19381-19386.
39. Li X, Lipowsky R, Kierfeld J. Bifurcation of velocity distributions in cooperative transport of filaments by fast and slow motors. *Biophys J*. 2013;104(3):666-676.
40. Kunwar A, Vershinin M, Xu J, Gross SP. Stepping, strain gating, and an unexpected force-velocity curve for multiple-motor-based transport. *Curr Biol*. 2008;18(16):1173-1183.
41. Rogers AR, Driver JW, Constantinou PE, Kenneth Jamison D, Diehl MR. Negative interference dominates collective transport of kinesin motors in the absence of load. *Phys Chem Chem Phys*. 2009;11(24):4882-4889.
42. Schneider R, Korten T, Walter WJ, Diez S. Kinesin-1 motors can circumvent permanent roadblocks by side-shifting to neighboring protofilaments. *Biophys J*. 2015;108(9):2249-2257.
43. Hendricks AG, Holzbaur EL, Goldman YE. Force measurements on cargoes in living cells reveal collective dynamics of microtubule motors. *Proc Natl Acad Sci USA*. 2012;109(45):18447-18452.
44. Rai AK, Rai A, Ramaiya AJ, Jha R, Mallik R. Molecular adaptations allow dynein to generate large collective forces inside cells. *Cell*. 2013;152(1–2):172-182.
45. Reddy BJ, Mattson M, Wynne CL, et al. Load-induced enhancement of Dynein force production by LIS1-NudE in vivo and in vitro. *Nat Commun*. 2016;7:12259.
46. Andreasson JO, Milic B, Chen GY, Guydosh NR, Hancock WO, Block SM. Examining kinesin processivity within a general gating framework. *Elife*. 2015;4:e07403. https://doi.org/10.7554/eLife.07403
47. Yan X, Hoek TA, Vale RD, Tanenbaum ME. Dynamics of translation of single mRNA molecules in vivo. *Cell*. 2016;165(4):976-989.
48. Altschuler SJ, Wu LF. Cellular heterogeneity: do differences make a difference? *Cell*. 2010;141(4):559-563.
49. Junker JP, van Oudenaarden A. Every cell is special: genome-wide studies add a new dimension to single-cell biology. *Cell*. 2014;157(1):8-11.
50. Woehlke G, Ruby AK, Hart CL, Ly B, Hom-Booher N, Vale RD. Microtubule interaction site of the kinesin motor. *Cell*. 1997;90(2):207-216.
51. Kunwar A, Tripathy SK, Xu J, et al. Mechanical stochastic tug-of-war models cannot explain bidirectional lipid-droplet transport. *Proc Natl Acad Sci USA*. 2011;108(47):18960-18965.
52. Edelstein A, Amodaj N, Hoover K, Vale R, Stuurman N. Computer control of microscopes using microManager. *Curr Protoc Mol Biol*. 2010;14:14.20.
53. Block SM, Asbury CL, Shaevitz JW, Lang MJ. Probing the kinesin reaction cycle with a 2D optical force clamp. *Proc Natl Acad Sci USA*. 2003;100(5):2351-2356.
54. Singh MP, Mallik R, Gross SP, Yu CC. Monte Carlo modeling of single-molecule cytoplasmic dynein. *Proc Natl Acad Sci USA*. 2005;102(34):12059-12064.
55. McKenney RJ, Vershinin M, Kunwar A, Vallee RB, Gross SP. LIS1 and NudE induce a persistent dynein force-producing state. *Cell*. 2010;141(2):304-314.

SUPPORTING INFORMATION

Additional Supporting Information may be found online in the supporting information tab for this article.

How to cite this article: Reddy BJN, Tripathy S, Vershinin M et al. Heterogeneity in kinesin function. *Traffic*. 2017;1–14. https://doi.org/10.1111/tra.12504

Heterogeneity in Kinesin function

Babu J N Reddy[1], Suvranta Tripathy[1,2], Michael Vershinin[3], Marvin Tanenbaum[4], Jing Xu[5], Michelle Mattson-Hoss[1], Karim Arabi[1], Dail Chapman[1], Tory Doolin[1], Changbong Hyeon[6‡], and Steven P. Gross[1‡]

[1]*Department of Developmental and Cell Biology, University of California,* Irvine, CA 92697.

[2]*Perelman School of Medicine, University of Pennsylvania,* Pennsylvania.

[3]*Department of Physics and Astronomy, University of Utah,* Salt Lake City, UT 84112.

[4]*Hubrecht Institute, The Royal Netherlands Academy of Arts and Sciences (KNAW)and University Medical Center* Utrecht, Uppsalaan 6, 3584CT Utrecht, The Netherlands.

[5]*School of Natural Sciences, University of California,* Merced, California 95343, USA*, and*

[6]*Korea Institute for Advanced Study,* Seoul 02455, Korea

[‡]Corresponding authors: *Changbong Hyeon, Email: hyeoncb@kias.re.kr and*

Steven P Gross, Email: sgross@uci.edu

Supplemental Information

Supplementary Information

Theory

Kinesin-1 “walks" processively along microtubules by converting chemical free energy of ATP into the motion along microtubules(1). Each realization of a kinesin time trace is a consequence of the cumulative sum of stochastic yet uncorrelated steps, where the waiting time between steps is drawn from an “independent and identically distributed" (i.i.d.) random variable whose distribution is given as a waiting time distribution, say, ψ(t). In this case, the “mean stepping time" from a motor time trajectory made of n steps is calculated as $\tau(n) = (1/n)\sum_{i=1}^{n} t_i$, where t_i is the dwell time between the (i -1)th and ith step. The mean stepping time, $\tau(n)$ should be identical for any motor as long as (i) all the motors are operated obeying the same law, and (ii) n is sufficiently large. When the mean velocity of the α^{th} kinesin is defined as, $V(n) = d/\tau_\alpha(n)$, where d (~ 8 nm) is the step size and $\tau_\alpha(n) = (1/n)\sum_{i=1}^{n} t_{\alpha.i}$ is the mean stepping time of the α^{th} motor, any kinesin molecule (α= 1,2,….N) is expected to have the identical mean velocity at long time (or sufficiently large number of steps, $n \to \infty$), i.e., $\lim_{n\to\infty} V_\alpha(n) = \bar{V}$.

To illuminate this point further, we consider an ensemble of Poisson walkers, by assuming that all the walkers obey the same rule: the waiting time distribution $\Psi(t) = \tau^{-1}e^{-t/\tau}$ for each step with τ=10 ms and step size d = 8 nm (Figure 1C). The positions of walkers along the track are expected to evolve as $\partial_t x(t) = \overline{V} + \eta(t)$ where η(t) is Gaussian white noise obeying $P[\eta(t)] \propto e^{-\int_0^t \frac{d\tau\eta^2(\tau)}{4\overline{D}}}$ with $\langle\eta(t)\eta(t')\rangle = 2\overline{D}\delta(t-t')$. Thus, the probability of finding a walker at position x at time t is $P[x(t)] = \left(4\pi\overline{D}\,t\right)^{-1/2}\exp\left[-(x(t)-\overline{V}\,t)^2/4\overline{D}\,t\right]$, and hence the mean velocity $\frac{x(t)}{t} = V(t)$ up to time *t* should obey the Gaussian-like velocity distribution

$$P_G[V(t)] = \left(\frac{t}{4\pi\overline{D}}\right)^{1/2} exp\left[-\frac{(V(t)-\overline{V})^2}{4\overline{D}/t}\right], \qquad [1]$$

where $\overline{V}$ and $\overline{D}$, in fact, can be expressed in terms of a single parameter τ as $\overline{V}(=\frac{d}{\tau} = 0.8\,\mu m/s)$ and $\overline{D} = d^2/2\tau(= 0.0032\,\mu m^2/sec)$.

Identification of components from individual kinesin molecules

The inconsistency of the assumption of homogeneous motor population with experimental data is already obvious among the individual time traces from the bead assays (Figure 1). In order to fully analyze the motion, we used the genetically labeled kinesin dataset (Figure 2, 4, 5 & 6). These experiments with fluorescently labeled kinesin assays not only gave more traces, but was perhaps closer to the in vivo case, because individual motors land spontaneously on MTs and start to move, rather than being brought into contact with the MT, as in the bead/optical trap assays. In qualitative agreement with the bead assay data, the time traces and $P(V)$ from TIRF-visualized kinesin data show the motor heterogeneity convincingly, with multiple peaks in velocity distribution. While on microtubule tracks, the slow motors are persistently slow, and the fast motors persistently fast; traces exhibiting slow-to-fast or fast-to-slow inter-conversion of velocity are definitely present,

but they are not dominant and was not included for our global, mean velocity analysis. The time traces presented in this study contradict the usual assumption of i.i.d., suggesting that not all the kinesin motors are functioning identically. Eq.3 that assumes homogeneity of motors fails to explain the P(V)s which displays multiple peaks both from the in vivo GFP-tagged K560 data (Figure 2) and the in vitro K560 data (Figure 3-7). P(V) in Figure 2, 3, 6 and 7 were fitted to a more generalized form assuming multiple components:

$$P_{hetero}(V) = \sum_{i=1}^{n} \phi_i P_{homo}(V; \overline{V}_i, \overline{D}_i, \overline{L}_i) \qquad (4)$$

Where $\sum_{i=1}^{n} \phi_i = 1$. The population of kinesins mapped on the velocity distribution is decomposed into multiple subpopulations.

	ϕ_1	ϕ_2	$\overline{V}_1$ $\mu m/sec$	$\overline{V}_2$ $\mu m/sec$
$K560_{24x}$gfp	0.7	0.3	1.24	0.6
15% Glycerol	0.96	0.04	0.39	0.17
30% Glycerol	1	0	0.21	n/a
pH 6.1	1	0	0.47	n/a
pH 6.4	1	0	0.54	n/a
pH 8.2	0.37	0.63	0.94	0.72
pH 10.8	0.27	0.73	1.00	0.76
34℃	0.72	0.28	0.80	0.40
37℃	0.80	0.20	0.90	0.45
23℃	0.64	0.36	0.71	0.40

Monte-Carlo Simulations with ε_{sAL} and ε_{nsAL} detachment for two motor cargos (Different Velocities)

When two motors on a cargo are separated by more than 100 nm, load is expected to be built up between them. For model ε_{nsAL}, the leading motor is subjected to opposing load, so its per-step detachment probability increases, but the rear motor's processivity is unaffected (since it is under forward load). The slow motor thus

interferes with the fast motor's processivity (**Supplemental Figure 5**); such interference is minimal when they have the same velocity (**Supplemental Figure 5D**, far right bar). Under these assumptions, a bead moved by two motors, each with v =1 μm/sec, L = 0.95μm, and an on-rate of 5/sec, will be transported on average of 3 μm before falling off the microtubule. This prediction agrees with our past theoretical model(2) under the same assumptions, and also with the mean field model(3). Importantly, here the predicted enhancement of travel distance for two motors relative to that for a single motor, was ~3.2. In contrast, for model 'ε_{sAL}', a load between motors will typically lead to detachment of the rear motor (due to assisting load from the fast motor) (**Supplemental Figure 5E**). Using these two models with different off-rate dependence on the forward load, we simulated heterogeneous pairs of motors on beads, with the velocity of the `fast' motor fixed at 1 μm/sec, and that of 'slow' motor varied from 0.1 to 1.0 μm/sec. The mean cargo run-lengths and mean cargo velocities extracted from simulations are shown in Figure 8C and **Supplemental Figure 5F**. By quantifying the function of the slow and fast motors in the presence of the other motor, we also determined how the motors interacted. As expected, for model 'ε_{sAL}', the larger the velocity difference between the two motors, the shorter the mean run-lengths of the slow motors; but the faster motors' processivity was unaffected (**Supplemental Figure 5E**). In contrast, for model 'ε_{nsAL}', larger velocity differences had no effect on single-motor processivity of the slow motor, but did decrease the faster motors' processivity (**Supplemental Figure 5D**). To confirm that the slow motors' short travel distances were due to the load from the faster forward motor, we did a set of control simulations where we gradually decreased the mean velocity of the fast motor while fixing the slow motors' velocity. As expected, as the fast motors' velocity decreased, the mean run-length of the slower motor increased (**Supplemental Figure 5B**), confirming our hypothesis. For model 'ε_{nsAL}', the slow motor acted as a brake, and the slower the slow motor with processivity of ~0.95μm, the greater the mean cargo travel distance as the fast motor gets more chances to rebind (Figure 8C, ε_{nsAL}). Thus, increased heterogeneity leads to slower, longer travel distance. In contrast, for model 'ε_{sAL}', slow motors detach rapidly and provide less drag but also contribute less to overall travel distance, so mean travel distance decreases with increasing velocity difference (Figure 8C, " ε_{sAL}). Overall, then, there is a functional trade-off (see discussion in the main text).

1. Visscher K, Schnitzer MJ, & Block SM (1999) Single kinesin molecules studied with a molecular force clamp. *Nature* 400(6740):184-189.
2. Kunwar A, Vershinin M, Xu J, & Gross SP (2008) Stepping, strain gating, and an unexpected force-velocity curve for multiple-motor-based transport. *Curr Biol* 18(16):1173-1183.
3. Klumpp S & Lipowsky R (2005) Cooperative cargo transport by several molecular motors. *Proceedings of the National Academy of Sciences of the United States of America* 102(48):17284-17289.

Supplemental Figure 1. Computer – generated time traces (N=1000) by using stepping time distributions: $\psi(t) = \tau^{-1}e^{-t/\tau}$ where $\tau = 10\ msec$ and step size $\mathrm{d} = 8\ nm$ are used. The histogram of mean velocity is fitted to Eq.1 in the main text with $\bar{V} = 0.8\ \mu m/sec$ and $\bar{D} = 0.0032\ \mu m^2/sec$ at *t*= 10 sec. P(V)s at *t*=2 and 50 sec are also plotted.

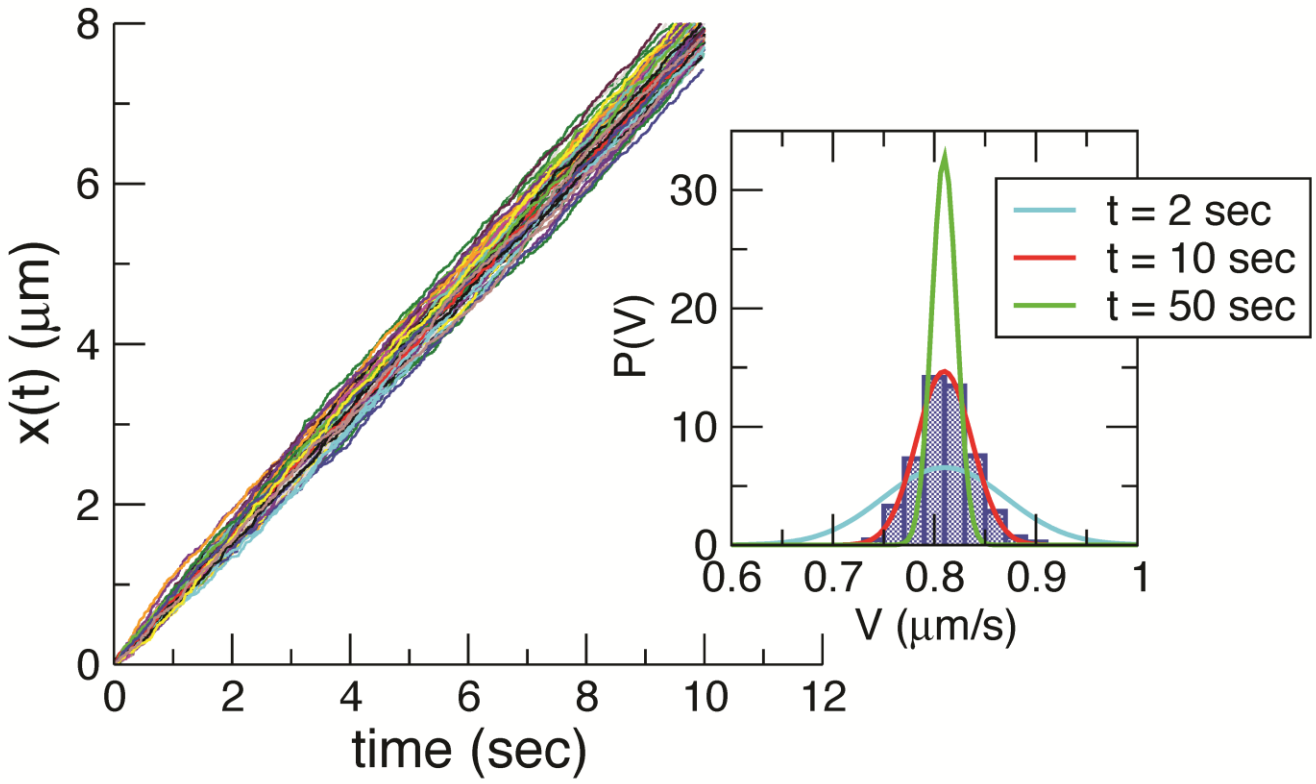

Supplemental Figure 2. Geometry and calibration of o-surface (elevated MT) measurements. (a) Diagram of experimental apparatus, showing location of cylindrical lens (CL) in front of camera, to induce distortion when the QD is out of focus. (b) Diagram of experimental geometry. Half-micron beads coated with mutant kinesin (which rigor-binds to MTs) are attached to the coverslip, and microtubules are subsequently owed in, and stick to the beads, ending up suspended between beads above the surface. (c) Quantification of asymmetry in QD image, as a function of the QDs distance from the plane of focus. The extent of asymmetry was used to detect QDs moving on MTs either close to or far-from the surface. The error bars are SEM, estimated by tracking the position and intensity profiles of 20 QDs in the time lapse images recorded during piezo motion.

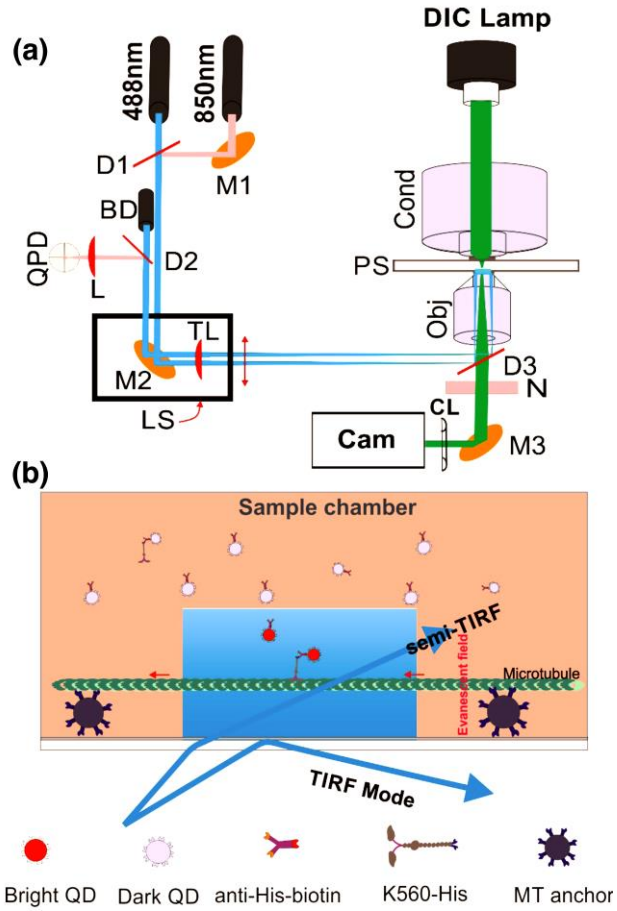

Supplemental Figure 3. Kinesin-560-gfp single molecule run lengths increase with pH.

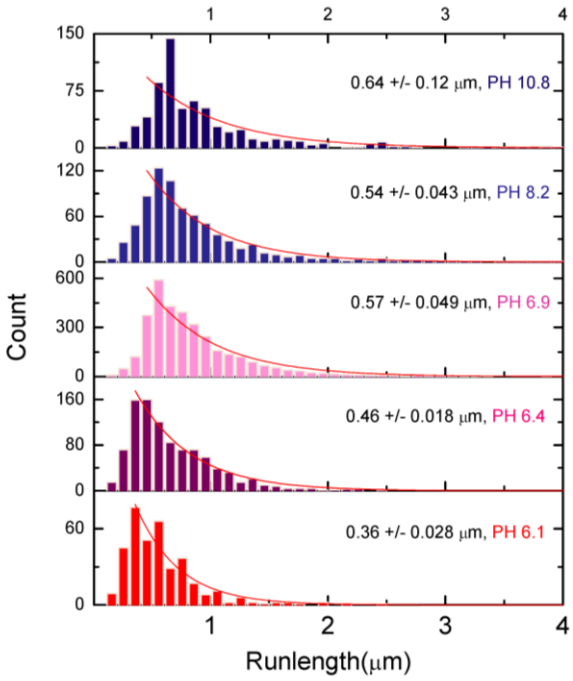

Supplemental Figure 4. Kinesin-560-gfp single molecule run lengths increase with temperature.

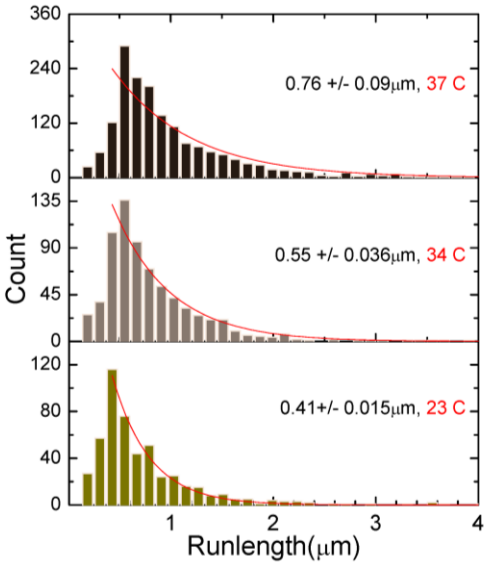

Supplemental Figure 5. Monte-Carlo simulations of two motor groups. (A) & (B) Two slow motor travel farther than two fast motors. (C)Single motor processivity is independent of velocity. (D) In model "ε_{nsAL} slow motor processivity in the two motor group is unaffected where as it is highly reduced in the model "ε_{sAL}(E). (F) 2-motor cargo velocities are determined by the slow motor in the model "ε_{nsAL} whereas they are less affected by the slow motor in the model "ε_{sAL} (G) Simulated run length distributions obtained by feeding experimentally extracted velocities of K-560 in model "ε_{sAL}. (H)Average ensemble velocities are less affected by the velocity heterogeneity whereas the distributions are affected

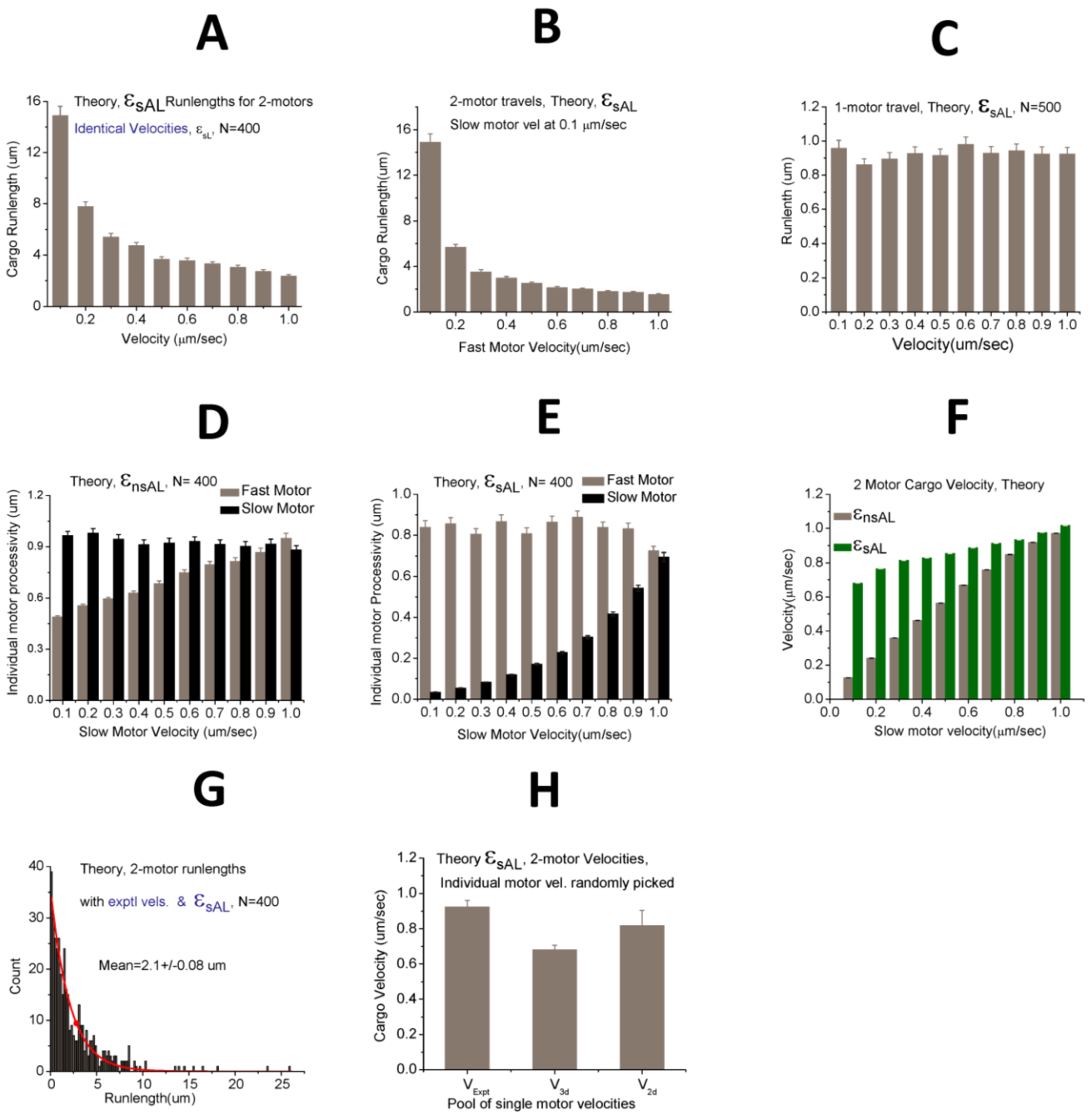

Supplemental Figure 6(A) Simulated average Velocities and Run lengths of 2-motor cargo under model 'ε_{sAL}'. For top 3 panels, the velocities were randomly chosen from the distributions in Figure. 8(D). (B) Average run-length of individual motors decreases with increasing number of motors on the cargo.